Arch. Comput. Meth. Engng.
Vol. **13, 4,** 471-513 (2006)

Archives of Computational Methods in Engineering
State of the art reviews

On Numerical Modelling of Growth, Differentiation and Damage in Structural Living Tissues

M. Doblaré

Group of Structural Mechanics and Materials Modelling
Aragón Institute of Engineering Research (I3A)
University of Zaragoza (Spain)
Campus Rio Ebro, Edif. Agustín de Betancourt
C/María de Luna, s/n. Zaragoza 50018, Spain
Email: mdoblare@unizar.es

J.M. García-Aznar

Group of Structural Mechanics and Materials Modelling
Aragón Institute of Engineering Research (I3A)
University of Zaragoza (Spain)
Campus Rio Ebro, Edif. Agustín de Betancourt
C/María de Luna, s/n. Zaragoza 50018, Spain

Summary

The main purpose of this work is to present a continuum formulation to model growth, differentiation and damage, valid for both hard and soft tissues. The governing equations follow the classical theory of multiphasic continuous media, including the influence of extracellular matrix composition and cell populations. Finally, this general framework is simplified and particularized to numerically simulate two important biological processes, such as, bone remodelling and bone fracture healing. These two simplified formulations have been implemented into a finite element context that allowed us to predict the evolution of the main aspects involved in such biological processes as growth, cell proliferation, migration, differentiation or death, and tissue pattern formation.

1 INTRODUCTION

It is well-known that tissue structure develops by a complex interaction between cells and their surrounding medium controlled by genetic instructions. The theoretical analysis of combined genetic and epigenetic development of living tissues (evo-devo models [1]) has become an important topic of research during the last years [2, 3]. One of the main factors that influences on this process is the mechanical environment, and thus, structural tissues are optimized in terms of their specific mechanical function [2]. This has motivated the appearance in the last years of many numerical models in order to better understand the interaction between mechanical and biological processes in developmental biology [2, 4]. Normally, these processes are classified according to their specific target into: remodelling, growth, differentiation, damage or healing models.

Remodelling describes the adaptive process by which the tissue modifies optimally its microstructure and hence its mechanical properties according to the mechanical environment that it supports. One of the most accepted hypotheses is that remodelling is activated with the goal of repairing the internal microdamage produced as a consequence of tissue function. An in depth review on this topic is presented in Section 3.1. Other extensive reviews may be found in [5, 6, 7].

Growth involves the addition or loss of mass, shaping the organs and adjusting their final dimensions. Hard tissues, such as bone, undergo only small deformations and growth is the result of surface mass apposition. On the contrary, soft tissues such as blood vessels or

 ISSN: 1134–3060 Received: June 2005

ligaments experience large deformations and suffer volumetric growth that leads to internal residual stresses. The kinematics of growth was firstly described mathematically by Skalak *et al.* in their milestone work [8]. Growth and deformation were there formulated as a sequence of two mappings: one representing load-free growth and the other the deformation due to the actual forces acting on the tissue. An extensive review of the most significant work in this field may be found in [9, 10, 2].

Tissue *differentiation* describes the differentiation to the various cell types from a non-specialized cell source [2, 4]. An extensive revision of the works that have been focused on modelling this biological process is made in Section 4.1.

Partial or total tissue *damage* is quite common. It can be caused by the sudden appearance of an overload that exceeds tissue strength, or by cyclic loads that gradually accumulate damage at a rate that cannot be repaired by tissue remodelling. After global tissue disruption *healing* is activated, with many cellular events involved [11, 12]. Healing is one of the most complete biological events, usually implying the appearance of tissue differentiation, growth and remodelling at the same time in a combined way. Not many numerical models have been developed to study this process, and most of them have been only focused on particular aspects as growth or differentiation. Nevertheless, a full revision is later performed in Section 4.1.

Although, as expressed above, most models have been developed to model specific biological processes, these events do not occur separately, but simultaneously. Therefore, their combined analysis requires to formulate more general models. Several works with strong theoretical fundamentals have been recently developed in this field. For example, Lubarda and Hoger [13] proposed a formulation of the mechanics of solids with a growing mass, into the global framework of finite deformation continuum thermodynamics. Kuhl and Steinmann presented a theoretical and numerical model for open system thermodynamics with application to hard tissues [14] and healing [15]. Garikipati *et al.* [16] proposed a complete formulation for mass transport and multiphasic mechanics in living tissues including growth.

In these formulations tissues are described from a macroscopic view point as a continuum mixture of cells and different types of extracellular matrices (ECMs) composed by fluid and several solid aggregates [2]. They give structural support to the tissue and provide cells with nutrients and signals including deformation and flow-induced stresses. These ECMs are produced by the cells and secreted into the surrounding medium.

The interaction between ECM and cell populations influences the dynamics of ECM accumulation and cell biological processes (proliferation, migration or differentiation) [17] [18] [19]. Some models have been developed that partially take into account these effects. Oster *et al.* [17] proposed a theoretical model in which mechanical interactions between cells and extracellular matrix determined growth patterns. Manoussaki [18] developed a numerical model to simulate the basic features of two mechanisms of blood vessel formation (angiogenesis and vasculogenesis), showing that mechanical interaction between endothelial cells and ECM is necessary to predict realistic results. In a similar way, Namy *et al.* [19] presented a computer model in which mechanical interactions of endothelial cells with extracellular matrix influence both active cell migration and cellular traction forces. They were able to reproduce several features of the tubulogenesis morphogenetic process *in vitro*. More recently Ramtani [20] developed a theoretical model to simulate wound healing, proposing that the wound contraction mechanism is not exclusively due to cell-ECM interaction forces but rather to both ECM-cell and cell-cell interactions.

In this work, we propose a more general continuum formulation for tissue growth, differentiation and damage, controlled by the mechanical environment, and that includes the main biological processes associated to each specialized cell population. We consider as independent variables those associated to the extracellular matrix (volumetric fractions,

damage degree, intrinsic density), cells (population densities) and growth kinematics. We establish all the typical governing equations in the context of continuum mixture theory (continuity, momentum principles, energy balance and entropy inequality), coupling mechanics, mass transport and cell dynamics. Finally, two applications: bone remodelling and bone fracture healing, including their numerical implementation and some examples are presented. We will show that the general formulation presented in this work can be used to formulate and simulate these two biological process.

The paper is organized as follows. Section 2 treats the fundamental balance equations for mass and cells and the kinematics of growth. In Section 3 we particularize this general formulation to the bone remodelling process, whereas in Section 4 we apply it to the healing course of a fracture. In each of these two cases we comment a numerical example and include additional references. Finally, a discussion and some concluding remarks are included in the last Section 5.

2 GLOBAL FRAMEWORK

We consider each tissue composed of N species (different tissue components and fluid) and M types of cells (normally each of them is related to one specie). We identify one of the species as the kinematic reference, while the rest are allowed to move relatively with respect to it.

We define the concentration (apparent density) of each specie ρ_0^i as mass of such specie at current time per unit total volume in the initial reference configuration Ω_0. This variable can also be expressed as $\rho_0^i = \overline{\rho}_0^i(V_m^i - h_0^i)$, being $\overline{\rho}_0^i$ the real tissue density, V_m^i the volume fraction of specie i with respect to the initial volume and h_0^i a scalar variable that quantifies the volume fraction of microcracks per unit total volume in the initial configuration within the specie i, both at current time. In the same way, we define the cellular concentration of each cell type j in Ω_0 as c_0^j.

We can also express the different variables in the current configuration Ω_t. Here, the concentrations of the species would be denoted by ρ^i and the cellular concentrations by c^i. The previous volume fractions in the reference and in the current states are related through the expression:

$$Jv_m^i = V_m^i \tag{1}$$

$$Jh^i = h_0^i \tag{2}$$

where $J = det(\boldsymbol{F})$, being $\boldsymbol{F}$ the deformation gradient associated to the reference volume with respect to which the different species diffuse and h^i the microcrack volume fraction in specie i per unit volume in the current configuration. Moreover, summing over all the species it is clear that

$$\sum_i V_m^i = 1 \tag{3}$$

$$J\sum_i v_m^i = \sum_i V_m^i = 1 \tag{4}$$

$$h_0 = \sum_i h_0^i \tag{5}$$

$$Jh = J\sum_i h^i = h_0 \tag{6}$$

with h_0 the total volume fraction of microcracks with respect to the initial total volume and h the one corresponding to the current volume.* In a similar way, we can relate the concentrations of species and cells in the initial and current configurations, that is, with respect to the initial and current total volumes, as:

$$\rho_0^i(\boldsymbol{X},t) = J\rho^i(\boldsymbol{x},t) = J\overline{\rho}_0^i(v_m^i - h^i) \tag{7}$$

$$c_0^i(\boldsymbol{X},t) = Jc^i(\boldsymbol{x},t) \tag{8}$$

2.1 Balance of Mass

The balance of mass in the reference configuration Ω_0 is stated as:

$$\frac{\partial \rho_0^i}{\partial t} = \frac{\partial \overline{\rho}_0^i}{\partial t}(V_m^i - h_0^i) + \overline{\rho}_0^i \frac{\partial V_m^i}{\partial t} - \overline{\rho}_0^i \frac{\partial h_0^i}{\partial t} = \Pi^i - \boldsymbol{\nabla}\cdot\boldsymbol{M}^i \qquad i = 1,...,N \tag{9}$$

and in the current configuration Ω_t

$$\frac{d\rho^i}{dt} + \rho^i \boldsymbol{\nabla}\cdot\boldsymbol{v} = \frac{d\overline{\rho}^i}{dt}(v_m^i - h^i) + \overline{\rho}^i \frac{dv_m^i}{dt} - \overline{\rho}^i \frac{dh^i}{dt} + \rho^i \boldsymbol{\nabla}\cdot\boldsymbol{v} = \pi^i - \boldsymbol{\nabla}\cdot\boldsymbol{m}^i \qquad i = 1,...,N \tag{10}$$

where Π^i, π^i are the net production of mass of the specie i per unit volume in the reference and current configurations respectively, $\boldsymbol{M}^i, \boldsymbol{m}^i$ the fluxes of transported mass of specie i per unit time and unit surface in the reference and current configurations respectively, related by the Piola transform $\boldsymbol{M}^i = J\boldsymbol{F}^{-1}\boldsymbol{m}^i$. Finally, $\frac{d}{dt}$ denotes the material time derivative and $\overline{\rho}^i(\boldsymbol{x}(\boldsymbol{X},t),t) = \overline{\rho}_0^i(\boldsymbol{X},t)$.

We have to keep in mind that biological processes are treated as open systems with respect to mass. Changes in mass can either be caused by local formation/resorption (net mass production) or mass diffusion (flux).† In fact, an open system is allowed to exchange mass, momenta, energy and entropy [14] with the exterior. In the particular case of assuming that new mass comes from the losses of other species (closed system with respect to mass) we could write:

$$\sum_i^N \pi^i = \sum_i^N \frac{\Pi^i}{J} = \frac{1}{J}\sum_i^N \Pi^i = 0 \Rightarrow \sum_i^N \pi^i = \sum_i^N \Pi^i = 0 \tag{11}$$

Moreover, the fluid is usually assumed to be incompressible and with no microcracks. This implies

$$\frac{\partial \bar{\rho}_0^f}{\partial t} = 0 \quad h_0^f = 0 \tag{12}$$

and, therefore,

$$\bar{\rho}_0^f \frac{\partial V_m^f}{\partial t} = \Pi^f - \boldsymbol{\nabla}\cdot\boldsymbol{M}^f \tag{13}$$

or

$$\bar{\rho}^f \frac{dv_m^f}{dt} + \rho^f \boldsymbol{\nabla}\cdot\boldsymbol{v} = \pi^f - \boldsymbol{\nabla}\cdot\boldsymbol{m}^f \tag{14}$$

*Soft tissues are usually assumed to be saturated and incompressible so $J = 1$ and therefore $\sum_i v_m^i = 1$. On the contrary, hard tissues are porous and its change of volume is mainly associated to changes in porosity due to mass apposition or resorption.

†Flux of species is allowed through material surfaces as it is evident for the fluid phase.

From Eq.(9) it becomes clear that the rate of volume fraction of each specie $\frac{\partial V_m^i}{\partial t}$ is determined from the net mass production Π^i, the flux of mass $\boldsymbol{M}^i$, the real tissue density evolution $\frac{\partial \overline{\rho}_0^i}{\partial t}$ and the rate of microcrack volume $\frac{\partial h_0^i}{\partial t}$. Next, we specify the evolution of each of these variables.

2.1.1 Production of mass

We assume that the production of mass, without taking into account the species actual density variation, is due to the activity of cells on that specie. Thus, we propose the expression:

$$\Pi^i - \frac{\partial \overline{\rho}_0^i}{\partial t}(V_m^i - h_0^i) = \sum_{j=1}^{M} c_0^j B_j^i \bar{\rho}_0^i(\tau = 0) \tag{15}$$

where B_j^i is the net volume production of specie i by cells of j type per unit cell and unit time, being $\tau = t - t_{pr}$ and t_{pr} the time at which a certain amount of mass is newly produced. It is interesting to remark that in the case of dead cells, production and removing of volume is null, therefore $B_d^i = 0$.

Equivalently, this expression can be written in the current configuration

$$\pi^i - \frac{d\overline{\rho}^i}{dt}(v_m^i - h^i) = \sum_{j=1}^{M} c^j \beta_j^i \bar{\rho}^i(\tau = 0) \tag{16}$$

Normally, most growth models assume that real tissue density is kept constant during growth and remodelling [16]. However, there are tissues whose real density changes with time. One typical example is bone, where its extracellular matrix is mineralized in a process that can last 6 months or more [21]. Therefore this evolution, $\frac{\partial \overline{\rho}_0^i}{\partial t}$, has to be explicitly characterized to complete the model.

2.1.2 Damage growth and removal

Fatigue microdamage contributes to degrade mechanical properties in living tissues [22, 23, 24, 25, 26]. In fact, the microscopic measure of the density of internal microcracks h may be related to the macroscopic mechanical degradation. In the isotropic theory of Continuum Damage Mechanics [27, 28] this macroscopic degradation is normally quantified by means of a variable d_0, known as continuum damage variable, which is restricted to the interval $[0, 1)$. And thus, for any material that incorporates damage, the Helmholtz free-energy function is usually expressed as:

$$\Psi = \Psi(\boldsymbol{\varepsilon}, d_0) = (1 - d_0)\Psi_0(\boldsymbol{\varepsilon}) \tag{17}$$

where Ψ_0 is the effective strain-energy function of the undamaged or intact material [27, 28]. In the particular case of elastic materials, damage is experimentally related to the loss of stiffness by means of the expression

$$d_0 = 1 - \frac{E}{E_0} \tag{18}$$

where E_0 corresponds to a reference value of the elastic modulus associated to the ideal undamaged material.

We should remark that this isotropic approach is the most simple. In this case, damage is assumed to be uniformly distributed in all the spatial directions. However, damage may be distributed in preferential directions. In this case an anisotropic approach would be necessary, which could be easily extrapolated from the isotropic case, simply replacing the

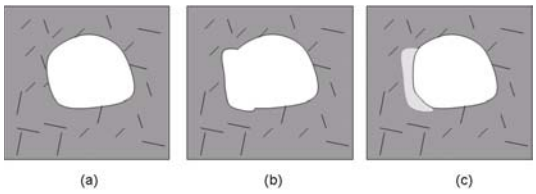

Figure 1. Schematic draw of how tissue remodelling repairs damage: (a) Initial distribution of microdamage. (b) Microdamage fraction per total volume after tissue resorption is reduced. (c) Microdamage fraction after new tissue formation remains constant

scalar d_0 by a second order tensor $\boldsymbol{d_0}$ [29]. In this paper, as a first approach, we have only focused on isotropic damage models.

Both variables d_0 and h_0 are physically related, although its relationship is yet not fully understood and depends on many factors, such as, load state, porosity, etc. In general, this relation can be expressed as:

$$f(d_0) = h_0 \tag{19}$$

Only particular correlations have been determined in bone tissue as for example that proposed by Burr *et al.* [30] that obtained a linear relationship between stiffness loss and crack effective area for intact canine femurs subjected to bending.

Contrary to inert materials, in living tissues, damage can be repaired, so the damage rate has to be expressed as a balance of damage growth and repair for each specie i:

$$\frac{\partial h_0^i}{\partial t} = \frac{\partial h_0^i}{\partial t}|_G - \frac{\partial h_0^i}{\partial t}|_R \tag{20}$$

Damage increase $\frac{\partial h_0^i}{\partial t}|_G$ is due to external mechanical loads that we consider independent of the biological processes involved. Therefore the definition of the corresponding evolution requires to know experimentally how damage accumulates with load. Damage repair $\frac{\partial h_0^i}{\partial t}|_R$ on the contrary is induced by remodelling or growth, being therefore clearly dependent on the biological processes developed within each specific specie by means of the evolution of $\frac{\partial V_m^i}{\partial t}$. As a first approach, we assume that damage h_0^i is uniformly distributed inside a representative macroscopic volume of the extracellular matrix and that damage repair is produced in a random way. Thus, when matrix is removed, damage is reduced, while when new undamaged matrix is deposited, damage is kept constant (see Figure 1). The mathematical law is then written as:

$$\frac{\partial h_0^i}{\partial t}|_R = \begin{cases} 0 & \text{if} \quad \dfrac{\partial V_m^i}{\partial t} \geq 0 \\ -\dfrac{\partial V_m^i}{\partial t}\dfrac{h_0^i}{V_m^i} & \text{if} \quad \dfrac{\partial V_m^i}{\partial t} < 0 \end{cases} \tag{21}$$

2.2 Balance of Cells

In a similar way, we define the balance of cells in the reference configuration Ω_0 as

$$\frac{\partial c_0^i}{\partial t} = \Pi_c^i - \boldsymbol{\nabla} \cdot \boldsymbol{M}_c^i \qquad i = 1, ..., M \tag{22}$$

and in the current configuration Ω_t

$$\frac{dc^i}{dt} + c^i \boldsymbol{\nabla} \cdot \boldsymbol{v} = \pi_c^i - \boldsymbol{\nabla} \cdot \boldsymbol{m}_c^i \qquad i = 1, ..., M \tag{23}$$

where, $c^i = c_0^i J^{-1}$ is the cell concentration of each cell type i (number of cells per unit volume) in the current configuration, $\pi_c^i = \Pi_c^i J^{-1}$ the net production of cells per unit volume and time in the current configuration, and finally, $\boldsymbol{m}_c^i = J^{-1}\boldsymbol{M}_c^i \boldsymbol{F}^T$ is the cell flux of type i per unit time and surface in the current configuration.

In this case, condition $\sum_i^M \pi_c^i = \sum_i^M \Pi_c^i = 0$ is never imposed since cells can proliferate as consequence of mitosis. We consider therefore the system always open with respect to cells. We have to remark that cell death is here considered as differentiation to a specific type of cell, so

$$\sum_i^M \Pi_c^i = \sum_i^M \Pi_{c_{pr}}^i \tag{24}$$

The net production of cells of type i can have different origins: proliferation, differentiation from different cells to this kind of cell or differentiation of this type of cell to other types (including dead cells). Thus, we can express the production of cells as:

$$\Pi_c^i = \Pi_{c_{pr}}^i + \sum_{j=1, j\neq i}^M c_0^j A_j^i - \sum_{j=1, j\neq i}^M c_0^i A_i^j \tag{25}$$

$$\Pi_c^i = \Pi_{c_{pr}}^i + c_0^i \sum_{j=1, j\neq i}^M (\frac{c_0^j}{c_0^i} A_j^i - A_i^j) = c_0^i [A_{pr}^i + \sum_{j=1, j\neq i}^M (\frac{c_0^j}{c_0^i} A_j^i - A_i^j)] \tag{26}$$

where $\Pi_{c_{pr}}^i$ is the production of cells of type i due to mitosis (proliferation) per unit time and volume in the initial configuration, A_{pr}^i is the same variable but per unit cell instead of per unit volume, and A_j^i is the generation of cells of type i due to differentiation of type j per unit cell j and per unit time. All these factors A_{pr}^i, A_j^i are dependent on the mechanical and biochemical environments. From the previous equation we conclude that:

$$\sum_{i=1}^M \Pi_c^i = \sum_{i=1}^M c_0^i A_{pr}^i \tag{27}$$

and

$$\sum_{i=1}^M c^i \sum_{j=1, j\neq i}^M (\frac{c_0^j}{c_0^i} A_j^i - A_i^j) = 0 \tag{28}$$

$$A_{pr}^d = 0 \tag{29}$$

$$A_d^i = 0 \ \forall i \tag{30}$$

2.2.1 Balance of linear momentum

We shall distinguish between the balance of linear momentum for species and for cells.

Let us start with the balance associated to each specie i in the reference configuration, Ω_0. The tissue is subjected to surface tractions, $\boldsymbol{T}$, such as, $\boldsymbol{T} = \sum_i \boldsymbol{P}^i \boldsymbol{N}$ on $\partial\Omega_0$, where $\boldsymbol{P}^i$ is the partial first Piola-Kirchhoff stress tensor corresponding to specie i, and body forces per unit mass, $\boldsymbol{G}$. We assume that all the species deform at each point with a common deformation gradient $\boldsymbol{F}$. The mass fluxes, $\boldsymbol{M}^i$, and mass sources, Π^i, also contribute to the balance of linear momentum. It is now convenient to define the material velocity of specie i relative to the reference phase as $\boldsymbol{V}^i = \frac{\boldsymbol{F}\boldsymbol{M}^i}{\rho_0^i}$. As fluxes are defined relative to the reference

phase, which does not diffuse, the total material velocity for each specie is $\boldsymbol{V}+\boldsymbol{V}^i$, being $\boldsymbol{V}$ the material velocity of the reference phase.

Taking into account all these considerations the balance of linear momentum of each specie i, written in integral form over Ω_0, becomes:

$$\begin{aligned}\frac{d}{dt}\int_{\Omega_0}\rho_0^i(\boldsymbol{V}+\boldsymbol{V}^i)dV &= \int_{\Omega_0}\rho_0^i\boldsymbol{G}dV+\int_{\Omega_0}\rho_0^i\boldsymbol{L}^i dV+\\ &+\int_{\Omega_0}\Pi^i(\boldsymbol{V}+\boldsymbol{V}^i)dV+\int_{\partial\Omega_0}\boldsymbol{P}^i\boldsymbol{N}dA-\\ &-\int_{\partial\Omega_0}(\boldsymbol{V}+\boldsymbol{V}^i)\boldsymbol{M}^i\cdot\boldsymbol{N}dA\end{aligned}\tag{31}$$

where $\boldsymbol{L}^i$ is the force per unit mass exerted upon specie i by all the other species and cells present in the tissue.

Next, we write the balance of linear momentum in the reference configuration, Ω_0, for the cell population j. In this case, we consider the mass of cells negligible, in comparison with the mass associated to the tissue. Therefore

$$\boldsymbol{0}=\int_{\Omega_0}c_0^j\boldsymbol{L}_c^j dV+\int_{\partial\Omega_0}\boldsymbol{P}_c^j\boldsymbol{N}dA\tag{32}$$

where $\boldsymbol{L}_c^j$ is the force per unit cell exerted upon cells j by the other species and cells present in the tissue and $\boldsymbol{P}_c^j$ is the first Piola-Kirchhoff stress tensor corresponding to the cell population j.

In the case of a closed system with respect to mass, summing over all species and cells, and taking into account that the change of momentum of the whole system is only affected by external agents, we can write

$$\sum_i\int_{\Omega_0}(\rho_0^i\boldsymbol{L}^i+\Pi^i(\boldsymbol{V}+\boldsymbol{V}^i))dV+\sum_j\int_{\Omega_0}c_0^j\boldsymbol{L}_c^j dV=\boldsymbol{0}\tag{33}$$

Taking into account the relation (11) for closed systems with respect to mass, we can obtain

$$\sum_i(\rho_0^i\boldsymbol{L}^i+\Pi^i\boldsymbol{V}^i)+\sum_j c_0^j\boldsymbol{L}_c^j=\boldsymbol{0}\tag{34}$$

Operating and localizing (31)(32) it is easy to obtain the differential version of the balance of linear momentum in the reference configuration for each specie i and cell population j:

$$\rho_0^i\frac{\partial(\boldsymbol{V}+\boldsymbol{V}^i)}{\partial t}=\rho_0^i(\boldsymbol{G}+\boldsymbol{L}^i)+\boldsymbol{\nabla}\cdot\boldsymbol{P}^i-[\boldsymbol{\nabla}(\boldsymbol{V}+\boldsymbol{V}^i)]\cdot\boldsymbol{M}^i\tag{35}$$

$$\boldsymbol{0}=c_0^j\boldsymbol{L}_c^j+\boldsymbol{\nabla}\cdot\boldsymbol{P}_c^j\tag{36}$$

Or equivalently, in the current configuration,

$$\begin{aligned}\rho^i\frac{d}{dt}(\boldsymbol{v}+\boldsymbol{v}^i) &= \rho^i(\boldsymbol{g}+\boldsymbol{l}^i)+\boldsymbol{\nabla}\cdot\boldsymbol{\sigma}^i-\\ &-[\boldsymbol{\nabla}(\boldsymbol{v}+\boldsymbol{v}^i)]\cdot\boldsymbol{m}^i-\rho^i[\boldsymbol{\nabla}\cdot(\boldsymbol{v}+\boldsymbol{v}^i)]\cdot(\boldsymbol{v}+\boldsymbol{v}^i)\end{aligned}\tag{37}$$

$$\boldsymbol{0} = c^j\boldsymbol{l}_c^j+\boldsymbol{\nabla}\cdot\boldsymbol{\sigma}_c^j\tag{38}$$

with no more than applying the push-forward operation weighted by J^{-1} to (35) (36) [31]. In (37)(38) $\boldsymbol{l}^i(\boldsymbol{x}(\boldsymbol{X},t),t)=\boldsymbol{L}^i(\boldsymbol{X},t)$, $\boldsymbol{l}_c^j(\boldsymbol{x}(\boldsymbol{X},t),t)=\boldsymbol{L}_c^j(\boldsymbol{X},t)$, $\boldsymbol{g}(\boldsymbol{x}(\boldsymbol{X}),t)=\boldsymbol{G}(\boldsymbol{x}(\boldsymbol{X}),t)$, $\boldsymbol{\sigma}^i=J^{-1}\boldsymbol{P}^i\boldsymbol{F}^T$ and $\boldsymbol{\sigma}_c^j=J^{-1}\boldsymbol{P}_c^j\boldsymbol{F}^T$.

2.2.2 Balance of angular momentum

For species, this balance is written as

$$\boldsymbol{P}^i \boldsymbol{F}^T = \boldsymbol{F} \boldsymbol{P}^{iT} \tag{39}$$

$$\boldsymbol{\sigma}^i = \boldsymbol{\sigma}^{iT} \tag{40}$$

both in the reference and deformed configurations respectively [16].

We now study this balance for the cell populations. The integral form of the balance of angular momentum written over Ω_0 for a cell population j is,

$$\mathbf{0} = \int_{\Omega_0} \boldsymbol{X} \times c_0^j \boldsymbol{L}_c^j dV + \int_{\partial\Omega_0} \boldsymbol{X} \times \boldsymbol{P}_c^j \boldsymbol{N} dA \tag{41}$$

Applying the divergence theorem gives

$$\mathbf{0} = \int_{\Omega_0} \boldsymbol{X} \times c_0^j \boldsymbol{L}_c^j dV + \int_{\Omega_0} \boldsymbol{X} \times \boldsymbol{\nabla} \cdot \boldsymbol{P}_c^j dV - \int_{\Omega_0} \boldsymbol{\varepsilon} : \boldsymbol{P}_c^j \tag{42}$$

where $\boldsymbol{\varepsilon}$ is the permutation symbol. Using now the balance of linear momentum for the cells j gives

$$\mathbf{0} = - \int_{\Omega_0} \boldsymbol{\varepsilon} : \boldsymbol{P}_c^j \tag{43}$$

Localizing this result and applying the properties of the permutation symbol we get the symmetry condition

$$\boldsymbol{P}_c^i \boldsymbol{F}^T = \boldsymbol{F} \boldsymbol{P}_c^{iT} \tag{44}$$

and, equivalently, for the Cauchy stresses

$$\boldsymbol{\sigma}_c^i = \boldsymbol{\sigma}_c^{iT} \tag{45}$$

2.2.3 Balance of energy

In addition to the terms previously introduced, some others have to be included. These are: E^i, the internal energy per unit mass of specie i; E_c^j, the internal energy per unit cell of cell type j; R^i, the heat supply to specie i per unit mass of that specie (we have not considered the heat supply to cells); and the heat flux vector i, $\boldsymbol{Q}^i$. All of them defined on Ω_0. Interaction energetic terms appear between species and cells: the energy per unit mass and unit time transferred to the specie i by all other species and cells, $\tilde{E}^i$; and the energy per unit cell transferred to the cell type j by all other species and cells, $\tilde{E}_c^j$. Working in the initial configuration Ω_0, we relate the rate of change of internal and kinetic energies of species and cells to the work done by mechanical loads, processes of mass/cell production and transport, heating and energy transfer:

$$\begin{aligned} \frac{d}{dt} \int_{\Omega_0} \rho_0^i (E^i + \frac{1}{2} \| \boldsymbol{V} + \boldsymbol{V}^i \|^2) dV = \int_{\Omega_0} (\rho_0^i \boldsymbol{G} \cdot (\boldsymbol{V} + \boldsymbol{V}^i) + \rho_0^i R^i) dV + \\ + \int_{\Omega_0} \rho_0^i \boldsymbol{L}^i \cdot (\boldsymbol{V} + \boldsymbol{V}^i) dV + \\ + \int_{\Omega_0} [\Pi^i (E^i + \frac{1}{2} \| \boldsymbol{V} + \boldsymbol{V}^i \|^2) + \rho_0^i \tilde{E}^i] dV + \\ + \int_{\partial\Omega_0} [(\boldsymbol{V} + \boldsymbol{V}^i) \cdot \boldsymbol{P}^i - \boldsymbol{M}^i (E^i + \frac{1}{2} \| \boldsymbol{V} + \boldsymbol{V}^i \|^2) - \boldsymbol{Q}^i] \boldsymbol{N} dA \end{aligned} \tag{46}$$

Note that we assume the internal energy only dependent of temperature, time and point and therefore production of new mass is assumed to have the same internal energy (in average) that the point where it appears

$$\frac{d}{dt}\int_{\Omega_0} c_0^j E_c^j dV = \int_{\Omega_0} c_0^j \boldsymbol{L}_c^j \cdot (\boldsymbol{V} + \boldsymbol{V}_c^j) dV + \int_{\Omega_0} (\Pi_c^j E_c^j + c_0^j \tilde{E}_c^j) dV + \\ + \int_{\partial\Omega_0} [(\boldsymbol{V} + \boldsymbol{V}_c^j) \cdot \boldsymbol{P}_c^j - \boldsymbol{M}_c^j E_c^j] \cdot \boldsymbol{N} dA \tag{47}$$

Applying the divergence theorem and using the balance of mass, balance of momenta and localizing the result, we have

$$\rho_0^i \frac{\partial E^i}{\partial t} = \boldsymbol{P}^i : \boldsymbol{\nabla}(\boldsymbol{V} + \boldsymbol{V}^i) - \boldsymbol{\nabla} \cdot \boldsymbol{Q}^i + \rho_0^i R^i + \rho_0^i \tilde{E}^i - \boldsymbol{\nabla} E^i \cdot \boldsymbol{M}^i \tag{48}$$

$$c_0^j \frac{\partial E_c^j}{\partial t} = \boldsymbol{P}_c^j : \boldsymbol{\nabla}(\boldsymbol{V} + \boldsymbol{V}_c^j) + c_0^j \tilde{E}_c^j - \boldsymbol{\nabla} E_c^j \cdot \boldsymbol{M}_c^j \tag{49}$$

Or equivalently in the current configuration

$$\rho^i \frac{de^i}{dt} = \boldsymbol{\sigma}^i : \boldsymbol{\nabla}(\boldsymbol{v} + \boldsymbol{v}^i) - \boldsymbol{\nabla} \cdot \boldsymbol{q}^i + \rho^i r^i + \rho^i \tilde{e}^i - \boldsymbol{\nabla} e^i \cdot \boldsymbol{m}^i - \rho^i [\boldsymbol{\nabla} \cdot (\boldsymbol{v} + \boldsymbol{v}^i)] e^i \tag{50}$$

$$c^j \frac{de_c^j}{dt} = \boldsymbol{\sigma}_c^j : \boldsymbol{\nabla}(\boldsymbol{v} + \boldsymbol{v}_c^j) + c^j \tilde{e}_c^j - \boldsymbol{\nabla} e_c^j \cdot \boldsymbol{m}_c^j - c^j [\boldsymbol{\nabla} \cdot (\boldsymbol{v} + \boldsymbol{v}_c^j)] e_c^j \tag{51}$$

In the case of a closed system with respect to mass, the inter-species energy transfer is related to interaction forces and mass sources, being therefore reduced to:

$$\sum_i (\rho_0^i \boldsymbol{L}^i \cdot \boldsymbol{V}^i + \Pi^i (E^i + \frac{1}{2} \| \boldsymbol{V}^i \|^2) + \rho_0^i \tilde{E}^i) + \sum_j (c_0^j \boldsymbol{L}_c^j \cdot \boldsymbol{V}_c^j + c_0^j \tilde{E}_c^j) = 0 \tag{52}$$

Summing (48) (49) over species i and cells j, respectively

$$\sum_i (\rho_0^i \frac{\partial E^i}{\partial t}) + \sum_j (c_0^j \frac{\partial E_c^j}{\partial t}) = \\ = \sum_i (\boldsymbol{P}^i : \dot{\boldsymbol{F}} + \boldsymbol{P}^i : \boldsymbol{\nabla} \boldsymbol{V}^i - \boldsymbol{\nabla} \cdot \boldsymbol{Q}^i + \rho_0^i R^i + \rho_0^i \tilde{E}^i - \boldsymbol{\nabla} E^i \cdot \boldsymbol{M}^i) + \\ + \sum_j (\boldsymbol{P}_c^j : \dot{\boldsymbol{F}} + \boldsymbol{P}_c^j : \boldsymbol{\nabla} \cdot \boldsymbol{V}_c^j + c_0^j \tilde{E}_c^j - \boldsymbol{\nabla} E_c^j \cdot \boldsymbol{M}_c^j) \tag{53}$$

being $\dot{\boldsymbol{F}} = \boldsymbol{\nabla} \boldsymbol{V}$. Substituting from Eq.(52), we finally obtain

$$\sum_i (\rho_0^i \frac{\partial E^i}{\partial t}) + \sum_j (c_0^j \frac{\partial E_c^j}{\partial t}) = \\ = \sum_i (\boldsymbol{P}^i : \dot{\boldsymbol{F}} + \boldsymbol{P}^i : \boldsymbol{\nabla} \boldsymbol{V}^i - \boldsymbol{\nabla} \cdot \boldsymbol{Q}^i + \rho_0^i R^i - \rho_0^i \boldsymbol{L}^i \cdot \boldsymbol{V}^i - \\ - \Pi^i (E^i + \frac{1}{2} \| \boldsymbol{V}^i \|^2) - \boldsymbol{\nabla} E^i \cdot \boldsymbol{M}^i) + \\ + \sum_j (\boldsymbol{P}_c^j : \dot{\boldsymbol{F}} + \boldsymbol{P}_c^j : \boldsymbol{\nabla} \boldsymbol{V}_c^j - c_0^j \boldsymbol{L}_c^j \cdot \boldsymbol{V}_c^j - \Pi_c^j E_c^j - \boldsymbol{\nabla} E_c^j \cdot \boldsymbol{M}_c^j) \tag{54}$$

This expression can also be written in the current configuration

$$\begin{aligned}
&\sum_i(\rho^i\frac{de^i}{dt})+\sum_j(c^j\frac{de^j_c}{dt})=\\
&=\sum_i(\boldsymbol{\sigma}^i:(\boldsymbol{d}+\boldsymbol{d}^i)-\boldsymbol{\nabla}\cdot\boldsymbol{q}^i+\rho^i r^i-\rho^i\boldsymbol{l}^i\cdot\boldsymbol{v}^i-\\
&\quad-\Pi^i(e^i+\frac{1}{2})(\|\boldsymbol{v}^i\|^2)-\boldsymbol{\nabla}e^i\cdot\boldsymbol{m}^i)+\\
&+\sum_j(\boldsymbol{\sigma}^j_c:(\boldsymbol{d}+\boldsymbol{d}^j_c)-c^j_0\boldsymbol{l}^j_c\cdot\boldsymbol{v}^j_c-\pi^j_c e^j_c-\boldsymbol{\nabla}e^j_c\cdot\boldsymbol{m}^j_c)-\\
&-\sum_i\rho^i e^i[\boldsymbol{\nabla}\cdot(\boldsymbol{v}+\boldsymbol{v}^i)]-\sum_j c^j e^j_c[\boldsymbol{\nabla}\cdot(\boldsymbol{v}+\boldsymbol{v}^j_c)]
\end{aligned}\tag{55}$$

with $\boldsymbol{d}=sym\boldsymbol{\nabla}\boldsymbol{v}$, $\boldsymbol{d}^i=sym\boldsymbol{\nabla}\boldsymbol{v}_i$ and $\boldsymbol{d}^j_c=sym\boldsymbol{\nabla}\boldsymbol{v}^j_c$.

2.2.4 The entropy inequality: Clausius-Duhem form

Let H^i be the entropy per unit mass of each specie i, H^j_c the entropy associated to the cell population per unit cell and Θ the absolute temperature. In this case, the entropy production inequality for the system as a whole is expressed as:

$$\begin{aligned}
&\sum_i\frac{d}{dt}\int_{\Omega_0}\rho^i_0H^idV+\sum_j\frac{d}{dt}\int_{\Omega_0}c^j_0H^j_cdV\geq\sum_i\int_{\Omega_0}(\Pi^iH^i+\frac{\rho^i_0R^i}{\Theta})dV+\\
&+\sum_j\int_{\Omega_0}\Pi^j_cH^j_cdV-\sum_i\int_{\partial\Omega_0}(\boldsymbol{M}^i\cdot\boldsymbol{N}H^i+\frac{\boldsymbol{Q}^i}{\Theta}\cdot\boldsymbol{N})dA-\sum_j\int_{\partial\Omega_0}\boldsymbol{M}^j_c\cdot\boldsymbol{N}H^j_cdA
\end{aligned}\tag{56}$$

Using the divergence theorem, the mass balance Eq.(9), the cellular balance Eq.(22) and localizing the resulting expression, we obtain the entropy inequality:

$$\begin{aligned}
&\sum_i(\rho^i_0\frac{\partial H^i}{\partial t})+\sum_j(c^j_0\frac{\partial H^j_c}{\partial t})\geq\\
&\geq\sum_i(\frac{\rho^i_0R^i}{\Theta}-\boldsymbol{\nabla}H^i\cdot\boldsymbol{M}^i-\frac{\boldsymbol{\nabla}\cdot\boldsymbol{Q}^i}{\Theta}+\frac{\boldsymbol{\nabla}\Theta\cdot\boldsymbol{Q}^i}{\Theta^2})-\sum_j(\boldsymbol{\nabla}H^j_c\cdot\boldsymbol{M}^j_c)
\end{aligned}\tag{57}$$

and in the current configuration

$$\begin{aligned}
&\sum_i(\rho^i\frac{d\eta^i}{dt})+\sum_j(c^j\frac{d\eta^j_c}{dt})\geq\\
&\geq\sum_i(\frac{\rho^ir^i}{\theta}-\boldsymbol{\nabla}\eta^i\cdot\boldsymbol{m}^i-\frac{\boldsymbol{\nabla}\cdot\boldsymbol{q}^i}{\theta}+\frac{\boldsymbol{\nabla}\theta\cdot\boldsymbol{q}^i}{\theta^2})-\sum_j(\boldsymbol{\nabla}\eta^j_c\cdot\boldsymbol{m}^j_c)-\\
&\quad-\sum_i(\rho^i\eta^i[\boldsymbol{\nabla}\cdot(\boldsymbol{v}+\boldsymbol{v}^i)])-\sum_j c^j\eta^j_c[\boldsymbol{\nabla}\cdot(\boldsymbol{v}+\boldsymbol{v}^j_c)])
\end{aligned}\tag{58}$$

Combining balance of linear momentum Eqs.(35) and (36), balance of energy (54) and

the entropy inequality multiplied by the absolute temperature Θ gives

$$\sum_i \rho_0^i(\frac{\partial E^i}{\partial t} - \Theta\frac{\partial H^i}{\partial t}) + \sum_j c_0^j(\frac{\partial E_c^j}{\partial t} - \Theta\frac{\partial H_c^j}{\partial t}) + \sum_i \Pi^i(E^i + \frac{1}{2}||\boldsymbol{V}^i||^2) +$$
$$+\sum_i \frac{\boldsymbol{\nabla}\Theta\cdot\boldsymbol{Q}^i}{\Theta} + \sum_i(\rho_0^i\frac{\partial}{\partial t}(\boldsymbol{V}+\boldsymbol{V}^i) - \rho_0^i\boldsymbol{G} - \boldsymbol{\nabla}\cdot\boldsymbol{P}^i + \boldsymbol{\nabla}(\boldsymbol{V}+\boldsymbol{V}^i)\cdot\boldsymbol{M}^i)\cdot\boldsymbol{V}^i -$$
$$-\sum_j(\boldsymbol{\nabla}\cdot\boldsymbol{P}_c^j)\cdot\boldsymbol{V}_c^j - \sum_i(\boldsymbol{P}^i:\dot{\boldsymbol{F}} + \boldsymbol{P}^i:\boldsymbol{\nabla}\boldsymbol{V}^i - (\boldsymbol{\nabla}E^i - \Theta\boldsymbol{\nabla}H^i)\cdot\boldsymbol{M}^i) -$$
$$-\sum_j(\boldsymbol{P}_c^j:\dot{\boldsymbol{F}} + \boldsymbol{P}_c^j:\boldsymbol{\nabla}\boldsymbol{V}_c^j - \Pi_c^jE_c^j - (\boldsymbol{\nabla}E_c^j - \Theta\boldsymbol{\nabla}H_c^j)\cdot\boldsymbol{M}_c^j) \le 0 \tag{59}$$

This expression is the reduced entropy inequality, also known as the Clausius-Duhem inequality, for this type of processes.

In the current configuration would be:

$$\sum_i \rho^i(\frac{de^i}{dt} - \theta\frac{d\eta^i}{dt} - (e^i - \theta\eta^i)[\boldsymbol{\nabla}\cdot(\boldsymbol{v}+\boldsymbol{v}^i)]) +$$
$$+\sum_j c_0^j(\frac{de_c^j}{dt} - \theta\frac{d\eta_c^j}{dt} - (e_c^j - \theta\eta_c^j)[\boldsymbol{\nabla}\cdot(\boldsymbol{v}+\boldsymbol{v}_c^j)])) +$$
$$+\sum_i \pi^i(e^i + \frac{1}{2}||\boldsymbol{v}^i||^2) + \sum_i \frac{\boldsymbol{\nabla}\theta\cdot\boldsymbol{q}^i}{\theta} +$$
$$+\sum_i(\rho^i\frac{d}{dt}(\boldsymbol{v}+\boldsymbol{v}^i) - \rho^i\boldsymbol{g} - \boldsymbol{\nabla}\cdot\boldsymbol{\sigma}^i + \boldsymbol{\nabla}(\boldsymbol{v}+\boldsymbol{v}^i)\cdot\boldsymbol{m}^i)\cdot\boldsymbol{v}^i - \sum_j(\boldsymbol{\nabla}\cdot\boldsymbol{\sigma}_c^j)\cdot\boldsymbol{v}_c^j -$$
$$-\sum_i(\boldsymbol{\sigma}^i:(\boldsymbol{d}+\boldsymbol{d}^i) - (\boldsymbol{\nabla}e^i - \theta\boldsymbol{\nabla}\eta^i)\cdot\boldsymbol{m}^i) -$$
$$-\sum_j(\boldsymbol{\sigma}_c^j:(\boldsymbol{d}+\boldsymbol{d}_c^j) - \pi_c^je_c^j - (\boldsymbol{\nabla}e_c^j - \theta\boldsymbol{\nabla}\eta_c^j)\cdot\boldsymbol{m}_c^j) \le 0 \tag{60}$$

2.2.5 The kinematics of growth

Literature on biological growth [8, 10] usually assumes that the total deformation gradient is multiplicatively decomposed into two terms, one corresponding to the growth tensor $\boldsymbol{F}^g$ which describes the amount and orientation of material added at each point, and the other to the true stress-related deformation tensor $\boldsymbol{F}^e$ that represents the deformation needed to accommodate the tissue to the addition of material during growth and also to the external loads [32]. In fact, the growth tensor $\boldsymbol{F}^g$ is, in general, incompatible.

As each specie i can grow in a different way, the growth tensor has to be defined for each of them through $\boldsymbol{F}^{g^i}$. Therefore, for each specie:

$$\boldsymbol{F} = \boldsymbol{F}^{e^i}\boldsymbol{F}^{g^i} \tag{61}$$

2.2.6 Constitutive relations from the Clausius-Duhem inequality

As usual in field theories of continuum physics, we use the Clausius-Duhem inequality (59) to obtain constitutive laws and thermodynamic constraints on the evolution of the different variables involved. It is usual to express the Clausius-Duhem inequality in terms of

the specific Helmholtz free energy Ψ. The specific internal energy is then expressed as $E^i = \Psi^i + \Theta H^i$ or equivalently for the cells $E^i_c = \Psi^i_c + \Theta H^i_c$. We assume that the material behaviour is elastic, fulfilling the axioms of locality, determinism, objectivity [31] and that the mass-specific Helmholtz free energy associated to each specie is a function of the tissue deformation tensor, temperature, specie density and damage $\Psi^i = \hat{\Psi}^i(\boldsymbol{F}^{e^i}, \Theta, \rho^i_0, d^i_0)$. Similarly, the cellular-specific Hemholtz free energy is defined as $\Psi^i_c = \hat{\Psi}^i_c(\boldsymbol{F}^{e^i}, \Theta, c^i_0)$. It is interesting to remark at this point that, since we consider cell populations from a macroscopic point of view, we assume that the cell free energy depends on the deformation tissue $\boldsymbol{F}^{e^i}$. Applying now the chain rule and regrouping terms, we get

$$
\begin{aligned}
&\sum_i (\rho^i_0 \frac{\partial \Psi^i}{\partial \boldsymbol{F}^{e^i}} - \boldsymbol{P}^i \boldsymbol{F}^{g^{iT}}) : \dot{\boldsymbol{F}}^{e^i} + \sum_j (c^j_0 \frac{\partial \Psi^j_c}{\partial \boldsymbol{F}^{e^j}} - \boldsymbol{P}^j_c \boldsymbol{F}^{g^{jT}}) : \dot{\boldsymbol{F}}^{e^j} + \sum_i \rho^i_0 (\frac{\partial \Psi^i}{\partial \Theta} + H^i) \frac{\partial \Theta}{\partial t} + \\
&+ \sum_j c^j_0 (\frac{\partial \Psi^j_c}{\partial \Theta} + H^j_c) \frac{\partial \Theta}{\partial t} + \sum_i \Pi^i (\Psi^i + \Theta H^i + \frac{1}{2} || \boldsymbol{V}^i ||^2) + \sum_i \rho^i_0 \frac{\partial \Psi^i}{\partial d^i_0} \dot{d}^i_0 + \\
&+ \sum_i \frac{\boldsymbol{\nabla} \Theta \cdot \boldsymbol{Q}^i}{\Theta} + \sum_i (\rho^i_0 \frac{\partial}{\partial t} (\boldsymbol{V} + \boldsymbol{V}^i) - \rho^i_0 \boldsymbol{G} - \boldsymbol{\nabla} \cdot \boldsymbol{P}^i + \boldsymbol{\nabla} (\boldsymbol{V} + \boldsymbol{V}^i) \cdot \boldsymbol{M}^i) \cdot \boldsymbol{V}^i - \\
&- \sum_j (\boldsymbol{\nabla} \cdot \boldsymbol{P}^j_c) \cdot \boldsymbol{V}^j_c - \sum_i [\boldsymbol{P}^i : (\boldsymbol{F}^{e^i} \dot{\boldsymbol{F}}^{g^i} + \boldsymbol{\nabla} \boldsymbol{V}^i) - (\boldsymbol{\nabla} \Psi^i + H^i \boldsymbol{\nabla} \Theta) \cdot \boldsymbol{M}^i] + \sum_i (\rho^i_0 \frac{\partial \Psi^i}{\partial \rho^i_0} \dot{\rho}^i_0) + \\
&+ \sum_j (c^j_0 \frac{\partial \Psi^j_c}{\partial c^j_0} \dot{c}^j_0) - \sum_j [\boldsymbol{P}^j_c : (\boldsymbol{F}^{e^j} \dot{\boldsymbol{F}}^{g^j} + \boldsymbol{\nabla} \boldsymbol{V}^j_c) - (\boldsymbol{\nabla} \Psi^j_c + H^j_c \boldsymbol{\nabla} \Theta) \cdot \boldsymbol{M}^j_c] + \\
&+ \sum_j \Pi^j_c (\Psi^j_c + \Theta H^j_c) \leq 0
\end{aligned}
\tag{62}
$$

Moreover, if we assume that in biological tissues the spatial temperature distribution is almost uniform ($\boldsymbol{\nabla} \Theta = \boldsymbol{0}$), expression (62) can be rewritten as

$$
\begin{aligned}
&\sum_i (\rho^i_0 \frac{\partial \Psi^i}{\partial \boldsymbol{F}^{e^i}} - \boldsymbol{P}^i \boldsymbol{F}^{g^{iT}}) : \dot{\boldsymbol{F}}^{e^i} + \sum_j (c^j_0 \frac{\partial \Psi^j_c}{\partial \boldsymbol{F}^{e^j}} - \boldsymbol{P}^j_c \boldsymbol{F}^{g^{jT}}) : \dot{\boldsymbol{F}}^{e^j} + \\
&+ \sum_i \rho^i_0 (\frac{\partial \Psi^i}{\partial \Theta} + H^i) \frac{\partial \Theta}{\partial t} + \sum_j c^j_0 (\frac{\partial \Psi^j_c}{\partial \Theta} + H^j_c) \frac{\partial \Theta}{\partial t} + \\
&+ \sum_i \Pi^i (\Psi^i + \Theta H^i + \frac{1}{2} || \boldsymbol{V}^i ||^2) + \sum_i \rho^i_0 \frac{\partial \Psi^i}{\partial d^i} \dot{d}^i + \\
&+ \sum_i (\rho^i_0 \frac{\partial}{\partial t} (\boldsymbol{V} + \boldsymbol{V}^i) - \rho^i_0 \boldsymbol{G} - \boldsymbol{\nabla} \cdot \boldsymbol{P}^i + \boldsymbol{\nabla} (\boldsymbol{V} + \boldsymbol{V}^i) \cdot \boldsymbol{M}^i) \cdot \boldsymbol{V}^i - \sum_j (\boldsymbol{\nabla} \cdot \boldsymbol{P}^j_c) \cdot \boldsymbol{V}^j_c - \\
&- \sum_i [\boldsymbol{P}^i : (\boldsymbol{F}^{e^i} \dot{\boldsymbol{F}}^{g^i} + \boldsymbol{\nabla} \boldsymbol{V}^i) - (\boldsymbol{\nabla} \Psi^i) \cdot \boldsymbol{M}^i] + \sum_i (\rho^i_0 \frac{\partial \Psi^i}{\partial \rho^i_0} \dot{\rho}^i_0) + \sum_j (c^j_0 \frac{\partial \Psi^j_c}{\partial c^j_0} \dot{c}^j_0) - \\
&- \sum_j [\boldsymbol{P}^j_c : (\boldsymbol{F}^{e^j} \dot{\boldsymbol{F}}^{g^j} + \boldsymbol{\nabla} \boldsymbol{V}^j_c) - (\boldsymbol{\nabla} \Psi^j_c) \cdot \boldsymbol{M}^j_c] + \\
&+ \sum_j \Pi^j_c (\Psi^j_c + \Theta H^j_c) \leq 0
\end{aligned}
\tag{63}
$$

Using standard arguments in continuum mechanics [33] and considering the behaviours of cells and species as independent, we easily obtain the following constitutive relations:

$$\boldsymbol{P}^i \boldsymbol{F}^{g^{iT}} = \rho_0^i \frac{\partial \Psi^i}{\partial \boldsymbol{F}^{e^i}} \tag{64}$$

$$\boldsymbol{P}_c^j \boldsymbol{F}^{g^{jT}} = c_0^j \frac{\partial \Psi_c^j}{\partial \boldsymbol{F}^{e^j}} \tag{65}$$

$$H^i = -\frac{\partial \Psi^i}{\partial \Theta} \tag{66}$$

$$H_c^j = -\frac{\partial \Psi_c^j}{\partial \Theta} \tag{67}$$

And the following constraints:

$$(\rho_0^i \frac{\partial \boldsymbol{V}}{\partial t} - \rho_0^i \boldsymbol{G} - \boldsymbol{\nabla} \cdot \boldsymbol{P}^i + (\boldsymbol{\nabla} \boldsymbol{V}) \cdot \boldsymbol{M}^i + \rho_0^i \boldsymbol{F}^{-T} \boldsymbol{\nabla} \Psi^i) \cdot \boldsymbol{V}^i \leq 0 \tag{68}$$

$$(c_0^i \boldsymbol{F}^{-T} \boldsymbol{\nabla} \Psi_c^i - \boldsymbol{\nabla} \cdot \boldsymbol{P}_c^i) \cdot \boldsymbol{V}_c^i \leq 0 \tag{69}$$

Eq.(64) specifies a constitutive relation for $\boldsymbol{P}^i \boldsymbol{F}^{g^{iT}}$ which corresponds to the elastic stress that the extracellular matrix (ECM) of each specie i experiences. Moreover, we also obtain the cellular stress $\boldsymbol{P}_c^j \boldsymbol{F}^{g^{jT}}$ that defines the combined effect of cell-ECM and cell-cell interaction [34] in terms of Ψ_c^j (see Eq.(65)).

The entropy H^i per unit mass of specie i is defined through Eq.(66) that corresponds to the definition usually employed in thermal physics. In a similar way, the entropy associated to cell populations per unit cell H_c^j is determined by Eq.(67).

The thermodynamic constraints derived from the Clausius-Duhem inequality are normally fulfilled by means of phenomenological constitutive relations. A clear example is the constitutive equation of heat conduction, that has been here removed due to the assumption of uniform temperature. And thus, from constraint (68) the following constitutive equation was originally proposed by Garikipati *et al.* [16] for species fluxes:

$$\rho_0^i \boldsymbol{V}^i = -\frac{\tilde{\boldsymbol{D}}^i}{\rho_0^i} (\rho_0^i \frac{\partial \boldsymbol{V}}{\partial t} - \rho_0^i \boldsymbol{G} - \boldsymbol{\nabla} \cdot \boldsymbol{P}^i + (\boldsymbol{\nabla} \boldsymbol{V}) \boldsymbol{M}^i + \rho_0^i \boldsymbol{F}^{-T} \boldsymbol{\nabla} \Psi^i) \tag{70}$$

with the constraint $\boldsymbol{w} \cdot \tilde{\boldsymbol{D}}^i \boldsymbol{w} \geq 0, \forall \boldsymbol{w} \in R^3$, being $\tilde{\boldsymbol{D}}^i$ the mobility tensor of specie i.

In a similar way, a phenomenological constitutive equation can be proposed from constraint (69) as

$$\boldsymbol{M}_c^i = -\boldsymbol{H}^i (\boldsymbol{\nabla} \Psi_c^i - (\boldsymbol{\nabla} \cdot \boldsymbol{P}_c^i) \cdot \frac{\boldsymbol{F}}{c_0^i}) \qquad , \boldsymbol{w} \cdot \boldsymbol{H}^i \boldsymbol{w} \geq 0, \forall \boldsymbol{w} \in R^3 \tag{71}$$

or equivalently

$$c_0^i \boldsymbol{V}_c^i = -\frac{\boldsymbol{H}^i}{c_0^i} (c_0^i \boldsymbol{F}^{-T} \boldsymbol{\nabla} \Psi_c^i - \boldsymbol{\nabla} \cdot \boldsymbol{P}_c^i) \qquad , \boldsymbol{w} \cdot \boldsymbol{H}^i \boldsymbol{w} \geq 0, \forall \boldsymbol{w} \in R^3 \tag{72}$$

In (71)(72) the cellular flux is defined as the product of a mobility tensor $\boldsymbol{H}^i$ (which is positive semi-definite) for each cell type and the corresponding thermodynamic driving force. The first term of this driving force represents that cells tend to move in the direction

contrary to their energy gradient, whereas the second term indicates the existence of a force that controls cell movement along $\boldsymbol{\nabla} \cdot \boldsymbol{P}_c^i$ [17].

With all these constitutive relations it is ensured the non-positiveness of certain terms of the entropy inequality, which is further reduced to

$$\begin{aligned}
&\sum_i [\rho_0^i \frac{\partial \Psi^i}{\partial \rho_0^i} \dot{\rho}_0^i - \boldsymbol{P}^i : (\boldsymbol{F}^{e^i} \dot{\boldsymbol{F}}^{g^i} + \boldsymbol{\nabla} \boldsymbol{V}^i)] + \sum_i \rho_0^i \frac{\partial \Psi^i}{\partial d_0^i} \dot{d}_0^i + \\
&+ \sum_i [\rho_0^i \boldsymbol{V}^i \cdot (\frac{\partial \boldsymbol{V}^i}{\partial t} + (\boldsymbol{\nabla} \boldsymbol{V}^i) \boldsymbol{F}^{-1} \boldsymbol{V}^i) + \Pi^i (\Psi^i + \Theta \frac{\partial \Psi^i}{\partial \Theta} + \frac{1}{2} \| \boldsymbol{V}^i \|^2)] + \\
&+ \sum_j [c_0^j \frac{\partial \Psi_c^j}{\partial c_0^j} \dot{c}_0^j - \boldsymbol{P}_c^j : (\boldsymbol{F}^{e^j} \dot{\boldsymbol{F}}^{g^j} + \boldsymbol{\nabla} \boldsymbol{V}_c^j) + \Pi_c^j (\Psi_c^j + \Theta \frac{\partial \Psi_c^j}{\partial \Theta})] \leq 0
\end{aligned} \tag{73}$$

In summary, the complete definition of this model requires to characterize the following functions for all the species: the production of mass Π^i by means of B_j^i (see Eq.(16)), the real tissue density evolution $\frac{\partial \overline{\rho}_0^i}{\partial t}$, the mechanical damage growth $\frac{\partial h_0^i}{\partial t}|_G$ and the mass-specific Helmholtz free energy Ψ^i; and for the cell populations: the production of cells Π_c^i by means of A_i^j, A_{pr}^i (see Eq.(26)), and finally, the cellular-specific Helmholtz free energy Ψ_c^i.

It is interesting to remark that in the particular case that all tissues are biphasic (one solid specie and fluid) and fully hydrated with no reference to cells, this general theory coincides with the classical biphasic poroelastic theory (see Appendix I).

3 A FIRST EXAMPLE OF APPLICATION: BONE REMODELLING

Bone tissue is a porous, heterogeneous and anisotropic material that adapts itself to the mechanical environment in order to get the maximum stiffness with the minimum weight. This adaptative process is known as bone remodelling. Nevertheless we have to keep in mind that bone mass homeostasis is not only determined by mechanical load, but also by calcium availability and sex steroids [35].

Bone remodelling is the coordinated result of two opposite processes of bone formation and resorption performed by teams of cells known as basic multicellular units (BMUs) that work on bone surfaces [36]. Resorption of bone by osteoclasts is followed by refilling of the resorption cavity by osteoblasts (additional details of the BMU activity are described in several works [21, 37]).

Many authors have described this bone activity by means of appropriate numerical models. Next, a review of the most significative is presented.

3.1 State of the Art of Computational Models on Bone Remodelling

From the 19th century many theoretical models have been proposed to explain how the mechanical environment influences on bone remodelling, being the "Wolff´s Law" the first of them [38]. With the development of faster computers and more reliable software, many of these theories have been tested and simulated using computational algorithms. This has motivated the development of many numerical models in the last years with the same objective of simulating the bone remodelling capacity [39, 40, 41, 42, 43, 44, 45, 46, 47].

Early formulations started with the *theory of adaptive elasticity* by Cowin and Hegedus [48] which was later used in a FEA simulation model by Hart *et al.* [49]. Adaptation of trabecular bone's apparent density based on isotropic behaviour and controlled by mechanical macroscopic variables, such as stress or strain, has been analyzed by different authors [39, 40, 50, 51]. Extensions to anisotropic behavior of this kind of models were

also performed by several authors [43, 44, 45, 46, 47]. More recently, several models of bone adaptation have been presented, based on the idea that remodelling is activated by microdamage with the aim of repairing it [41, 42, 52]. To obtain a deeper insight into these models, several authors have provided relevant overviews [5, 6].

Most of these adaptive models are purely phenomenological and explain the net increase or decrease of bone apparent density by the coordinated and simultaneous activity of osteoblasts and osteoclasts. However, more biologically-based models are necessary in order to take into account the effects of both biological and mechanical factors. In this sense, some attempts have been made in the last years [53, 37, 21, 54].

Actually, Huiskes *et al.* [53] proposed a model that includes a separate description of osteoclastic resorption and osteoblastic formation. A biological osteocyte mechanosensory system was employed in order to enable the simulation of remodelling in a *mechanobiological* way.

Hazelwood *et al.* [37] developed a model of mechanical adaptation with metabolic items of bone remodelling. Their model simulates the evolution of bone porosity by a two-stage process (resorption-formation) performed by BMUs. The rate of appearance of these units is calculated as a function of the bone tissue surface available for remodeling and the level of disuse and accumulated microdamage. Although this model established an important advance in understanding the remodelling process, it presents some limitations. In fact, it does not consider the three-dimensional geometry of BMU, but used a 2D approximation. Moreover, the process of mineral accumulation in newly osteoid bone volume, which plays an important role in bone remodelling as many authors have pointed out [55], was not taken into account. Additionally, the influence of the damage level on the macroscopic stiffness was also neglected, which itself alters the mechanical local stimulus and, therefore, influences on the remodelling process. Apart from these theoretical items, the model was only applied to simulate the porosity increase in cortical bone.

Hernandez, Beaupré and Carter [21, 54, 56] proposed a computational model of bone remodelling that considers the complete activity of BMUs from a three-dimensional point of view and accounts for changes in the degree of mineralization of bone tissue. Measurements taken from histomorphometric studies of human bone were used to represent the rate of appearance, shape, rate of progression and lifespan of BMUs as well as the time periods during which bone is resorbed and formed at each individual remodelling site. Although this model implied a significant advance in the comprehension and simulation of the bone remodelling process, it is certainly restricted. The theoretical formulation of this model considers a mechanical stimulus [21, 54] which was not employed in the numerical analyses. Furthermore, the impact of cumulative microdamage was neglected despite its significance indicated by many authors [41, 37, 22, 57].

More recently García-Aznar *et al.* [7] proposed a more extended computational model of bone remodelling considering that both mechanical and biological factors work in a couple way in order to control more efficiently the bone remodelling process. This model is, in fact, a particular case of the general formulation proposed in the first part of this paper. Therefore, we use it here as an example of application of this formulation.

3.2 Particularization of the General Formulation to Bone Remodelling

The model proposed by García-Aznar *et al.* [7] is based on the following simplificative assumptions with respect to the general formulation previously proposed:

1. In this case, instead of working with the concentration of bone cells, we use the same concentration but of BMUs.

2. We consider only one solid specie, obviously the reference phase, that corresponds to bone tissue with its specific cells (BMUs).

3. Due to the high stiffness of bone tissue, it is usual to work under the small strains assumption, hence current and initial configurations are coincident.

Next, the BMU balance, mass balance and growth equations are particularized for this specific example.

3.2.1 Balance of BMUs

In this case we define the balance of BMUs in the reference configuration Ω_0 as

$$\frac{\partial N_{BMU}}{\partial t} = \Pi_{BMU} = \Pi^{+}_{BMU} - \Pi^{-}_{BMU} \tag{74}$$

where N_{BMU} is the number of BMUs per unit volume in the reference configuration and Π_{BMU} is the net production of BMUs per unit volume and time in the reference configuration. Therefore, we assume as a first approach that the BMU flux is null $\boldsymbol{M}_{BMU} = \boldsymbol{0}$, that is the advance of BMUs is negligible with respect to the dimensions of the macroscopic reference volume.

Following the model proposed by García-Aznar *et al.* [7], the birth-rate of BMUs is determined by the law:

$$\Pi^{+}_{BMU}(t) = f_{bio}(1-s)S_v \tag{75}$$

where f_{bio} is a biological parameter that depends on factors like age, sex, nutrition, etc., S_v is a measurable variable that defines the available bone surface per unit bone volume that directly depends on bone porosity [58] and s is an inhibitory signal transmitted by the osteocytic network to the BMUs present on the bone surface. This signal is dependent on the strain level $\bar{\varepsilon}_i = \sqrt{\frac{2U}{E}}$ for each load case i, the number of applied cycles N_i and the damage level d, through the expression:

$$s(\bar{\varepsilon}, N, d) = \frac{(\sum_i N_i \bar{\varepsilon}_i^m)^{1/m}}{(\sum_i N_i \bar{\varepsilon}_i^m)^{1/m} + c}(1-d)^a \tag{76}$$

where m is an exponent that controls the influence of the strain amplitude versus the number of cycles, c is a constant that determines the influence of the mechanical usage and a is a parameter that weights the effect of damage in the inhibitory signal.

We also assume that BMUs die when they finish their activity, therefore

$$\int_0^t \Pi^{-}_{BMU}(t')dt' = \int_{-\sigma_L}^{t-\sigma_L} \Pi^{+}_{BMU}(t')dt' \tag{77}$$

where σ_L is the lifespan of a BMU and refers to the time during which the first appearing osteoclasts are active.

3.2.2 Balance of mass

In this case we only consider bone tissue. Thus, we obtain the following expression for the mass balance:

$$\frac{\partial \rho_0^b}{\partial t} = \frac{\partial \overline{\rho}^b}{\partial t}(V_m^b - h_0) + \overline{\rho}^b \frac{\partial V_m^b}{\partial t} - \overline{\rho}^b \frac{\partial h_0}{\partial t} = \Pi^b \tag{78}$$

where the temporal evolution of each variable is determined in an independent way. Next we justify the evolution of each term.

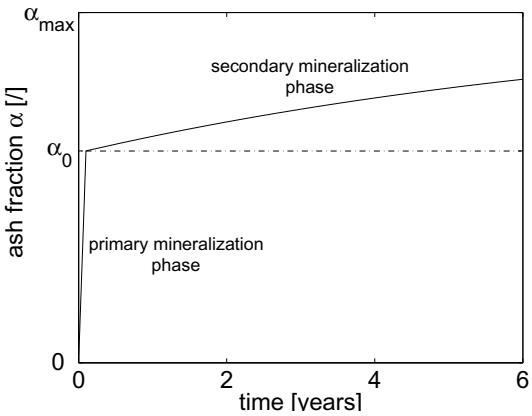

Figure 2. Evolution of the ash fraction with time. κ has been chosen such that 50 % of the secondary mineralization is achieved after 6 years

Firstly, we start with the term that defines the evolution of the real bone tissue density $\frac{\partial \overline{\rho}^b}{\partial t}$. Bone formation involves three different steps: production of the extracellular matrix (osteoid), primary mineralization of the matrix that occurs very quickly (in 6 days a 60% of the maximum mineral content is produced) and secondary mineralization that is very slow and takes 6 years or more. This process is basic in the determination of the mechanical properties of bone like elasticity modulus and strength. García-Aznar *et al.* [7] model the evolution of the real tissue density using an intermediate variable α (mineralization degree or ash fraction) that is experimentally correlated to the real tissue density through the following expression [21, 59]:

$$\bar{\rho}^b = 1.41 + 1.29\alpha \tag{79}$$

They assume that primary mineralization occurs immediately, while the mineralization rate during the secondary phase is

$$\alpha(t) = \alpha_{max} + (\alpha_0 - \alpha_{max})e^{-\kappa t} \tag{80}$$

where α_0 denotes the ash fraction resulting from the primary phase and α_{max} its maximum physiological value. The constant κ determines the velocity of this process (Figure 2).

As the degree of mineralization is not directly correlated with the bone volume fraction, an averaged ash fraction $\bar{\alpha}$ is introduced that takes into account the different mineralization stages of the remodelled bone

$$\bar{\alpha}(t) = \frac{(V_m^b(0) - h_0(0))\alpha(0) + \int_0^t \left((\dot{V}_F(\tau) - h_0(\tau))\alpha(t-\tau) - (\dot{V}_R(\tau) - h_0(\tau))\bar{\alpha}(\tau)\right) d\tau}{V_m^b(t) - h_0(t)} \tag{81}$$

where V_F and V_R are the volume ratios of created and resorbed bone respectively, during the bone remodelling process developed by the BMUs.

As previously explained, during BMU activity, bone is continuously renewed by resorption and formation, and therefore the bone volume fraction V_m^b changes depending on the

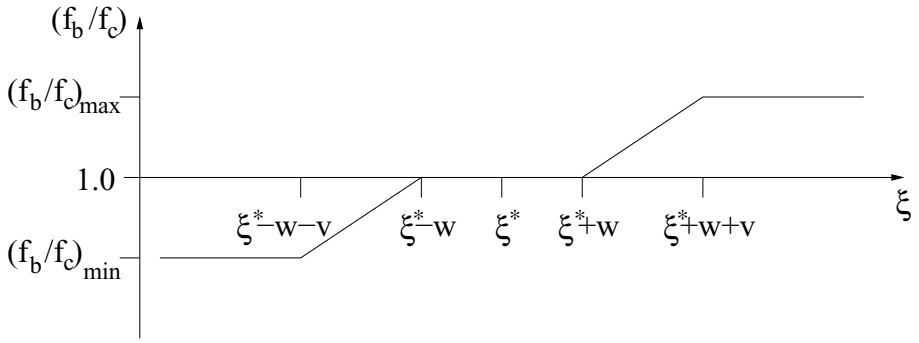

Figure 3. Model for the focal bone balance

different mechanical usages. We consider the following equations of evolution:

$$\dot{V}_F(t) = \int_{t-T_R-T_I-T_F}^{t-T_R-T_I} \left(\int_{t'-\sigma_L}^{t'} \Pi^+_{BMU}(t'')dt'' \right) \frac{A_{BMU}}{T_F} \frac{f_b}{f_c}(t') v_{BMU} dt' \tag{82a}$$

$$\dot{V}_R(t) = \int_{t}^{t-T_R} \left(\int_{t'-\sigma_L}^{t'} \Pi^+_{BMU}(t'')dt'' \right) \frac{A_{BMU}}{T_R} v_{BMU} dt' \tag{82b}$$

$$\dot{V}^b_m = \dot{V}_F - \dot{V}_R \tag{83}$$

where Π^+_{BMU} is the BMU birth-rate defined by Eq.(74), T_R, T_F and T_I are the resorption, formation and reversal periods respectively, v_{BMU} is the rate of progression of a BMU, A_{BMU} is the cross section of a BMU (distinguishing between cortical and trabecular bone) and $\frac{f_b}{f_c}(t')$ is the ratio between osteoblasts and osteoclasts activities that is assumed to be controlled by the mechanical stimulus $\xi = \sum_i N_i \bar{\varepsilon}_i^m$ by means of a standard law (see Figure 3) in remodelling models.

It is also considered that microcracks appear in bone as consequence of fatigue load, but this damage is repaired by bone remodelling. In fact, many authors consider that damage is the main stimulus that activates bone remodelling [37, 52, 41]. We also consider that damage has an important role in the activation of bone remodelling by means of expression (76). Therefore, the damage rate is the difference between damage accumulation by loads and damage repair by bone remodelling following the rule previously presented in (20).

As previously commented, microcrack density h_0 influences on the degradation of the mechanical properties of the tissue quantified by means of the variable damage d_0 defined in (18). The general expression that relates both variables (19) is in this example simplified to:

$$h_0 = k d_0 \tag{84}$$

with $k = 0.00034$ [30].

It has been experimentally observed that damage accumulation due to mechanical load is different for tension and compression [60]; for example, García-Aznar *et al.* [7] proposed a different evolution law depending on the load type. Moreover, since fatigue behaviour of bone subjected to cyclic loads is normally studied through the evolution of the degradation of the elastic modulus (d_0), it is usual to express the microcrack evolution in terms of this

variable:

$$\frac{\partial h_0}{\partial t}|_G = k\frac{\partial d_0}{\partial t}|_G = \begin{cases} k\dfrac{C_1}{\gamma_1}e^{\gamma_1 d_0}\tilde{\varepsilon}^{\delta_1} & \text{in compression} \\ k\dfrac{C_2}{C_3\gamma_2}(1-d_0)^{1-\gamma_2}e^{-C_3(1-d_0)^{\gamma_2}}\tilde{\varepsilon}^{\delta_2} & \text{in tension} \end{cases} \tag{85}$$

where all parameters C_j, γ_j and δ_j were determined from experiments of Pattin *et al.* [60].

Bone as living tissue is able to repair this damage. Assuming a uniform damage distribution and a random bone remodelling process, damage is reduced following the expression (21), or equivalently

$$\frac{\partial h_0}{\partial t}|_R = \begin{cases} 0 & \text{in formation} \\ -\dot{V}_R\dfrac{h_0}{V_m^b} & \text{in resorption} \end{cases} \tag{86}$$

3.2.3 Material behaviour

The material behavior in this model [7] is also simplified. Bone is considered to behave as linear elastic and heterogeneous, with the elasticity modulus depending on the bone volume fraction v_b, the mineralization ratio $\bar{\alpha}$, and the damage level d_0 through the rule:

$$E = 84370 v_b^{2.58}\bar{\alpha}^{2.74}(1-d_0)MPa \tag{87}$$

Additionally, we assume that the Poisson ratio is set to a constant value $\nu = 0.3$.

3.2.4 Numerical example

In a previous paper [7] several examples were developed in order to check the potential of the model to predict stress fractures and bone remodeling activated by disuse, overload and damage. Here, we review some of the most significative results. For example, we show (see Figure 4) the evolution of the bone volume fraction for different initial densities (2.05, 1.0 and 0.5 g/cm^3) under uniaxial constant strain applied for a fixed number of cycles per day (10,000 cycles/day), corresponding to different states of strain level: equilibrium ($\xi = \xi_0^*$), overload ($\xi = 2\xi_0^*$), high overload ($\xi = 7\xi_0^*$) and disuse ($\xi = 0$). For cortical bone (initial density of $2.05\, g/cm^3$) the model responds with a slight increase in bone volume fraction for overload, with a small decrease in the case of high overload due to microdamage accumulation and a higher reduction in case of disuse. However, for cancellous bone (initial density of 1.0 or 0.5 g/cm^3) a slight increase in bone volume fraction is produced under overload and high overload. The differences found in the response of bone under high overload are mainly due to the different levels of damage produced in each case (see Figure 5). In the case of cortical bone we can see how damage increases very quickly and later it is repaired by means of bone remodelling activation and consequent bone resorption. For trabecular bone the level of damage is so small that it does not activate bone remodelling, and therefore damage continuously increases without loss of bone volume.

Finally, this model has been also used to study the bone remodeling induced by the implantation of a hip prosthesis. Specific description of this numerical simulation can be found in the work of García-Aznar *et al.* [7]; here we only review the main results obtained. We can see in Figure 6 the initial distribution of bone volume fraction considered in the intact femur, the mesh of the prosthesis that is implanted and the corresponding evolution of the bone volume fraction predicted with this model.

For the two biological factors f_{bio} considered, femoral adaptive bone remodelling occurs over the entire bone that surrounds the fixation, although the main bone loss was obtained proximally and this loss decreases from the proximal to the distal area. Obviously a higher

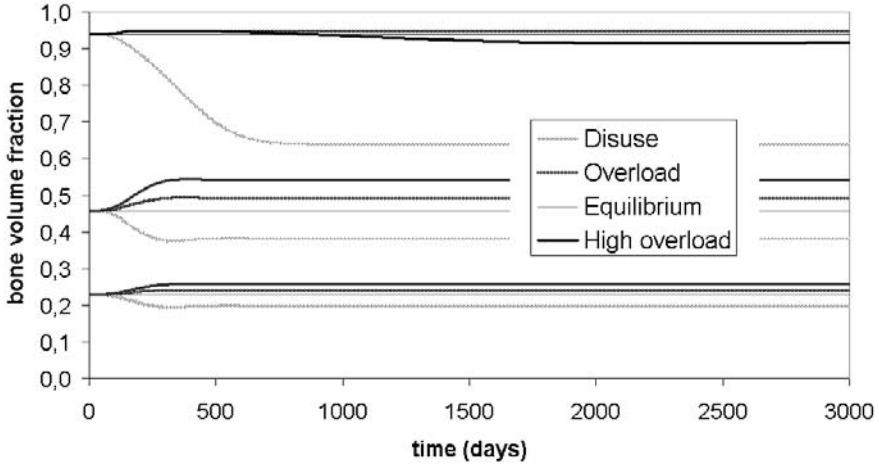

Figure 4. Evolution of the bone volume fraction for different initial densities, $\rho_0 =$ 2.05, 1.0, and $0.5\,g/cm^3$ (all with reference to an initial ash fraction of 0.6), and for states of equilibrium $\xi = \xi_0^*$, overload $\xi = 2\xi_0^*$, high overload $\xi = 7\xi_0^*$ and disuse $\xi = 0$. [7]

biological factor f_{bio} causes a higher bone loss. Moreover we found that after the second year of simulation, bone loss was minimal. Both facts have been also determined clinically in similar regions and for comparable periods of time [61].

4 A SECOND EXAMPLE OF APPLICATION: BONE FRACTURE HEALING

Bone fracture healing is a regenerative biological response of bone to traumatic bone lesions in order to restore its original integrity. A bone fracture causes haemorrhage and tissue disruption. This damaged tissue is normally known as debris tissue and its spatial distribution is fully dependent on how the fracture is produced. Later, a complex cellular process is activated consisting of inflammation, growth, tissue differentiation, ossification and remodelling. Initially, within the first few days after fracture, the inflammatory process begins to remove debris from the fracture site and to form a hematoma. At the same time, fibroblasts proliferate and capillary sprouts grow into blood clot in the injured area, forming granulation tissue in response to cytokines released by tissue damage. The role of this new formed tissue is very important because allows the invasion of mesenchymal stem cells to the fracture site. But, although this reparative process starts, if the fracture is not completely stabilized, the movement continues causing additional disruption to this granulation tissue, altering the normal reparative process and leading to a non-union or delayed union. If the stability is sufficient, stem cells start to differentiate into osteoblasts forming intramembranous woven bone adjacent to bone and distal to the fracture. Later, bone and cartilage are produced in different parts of the callus, as a consequence of stem cell differentiation into osteoblasts and chondrocytes. At the same time, the intramembranous ossification front advances to the centre of the callus. After this, the endochondral ossification process starts with cartilage calcification and replacement with new bone. When the bony bridge closes the fracture gap, bone reunion is produced in this region. Finally, the external callus is fully resorbed and the woven bone in the gap is remodelled into organised cortical bone. All these processes that appear during this complex regenerative event depend directly on the relative movement between the bone fragments. In fact, bone is formed directly in absence

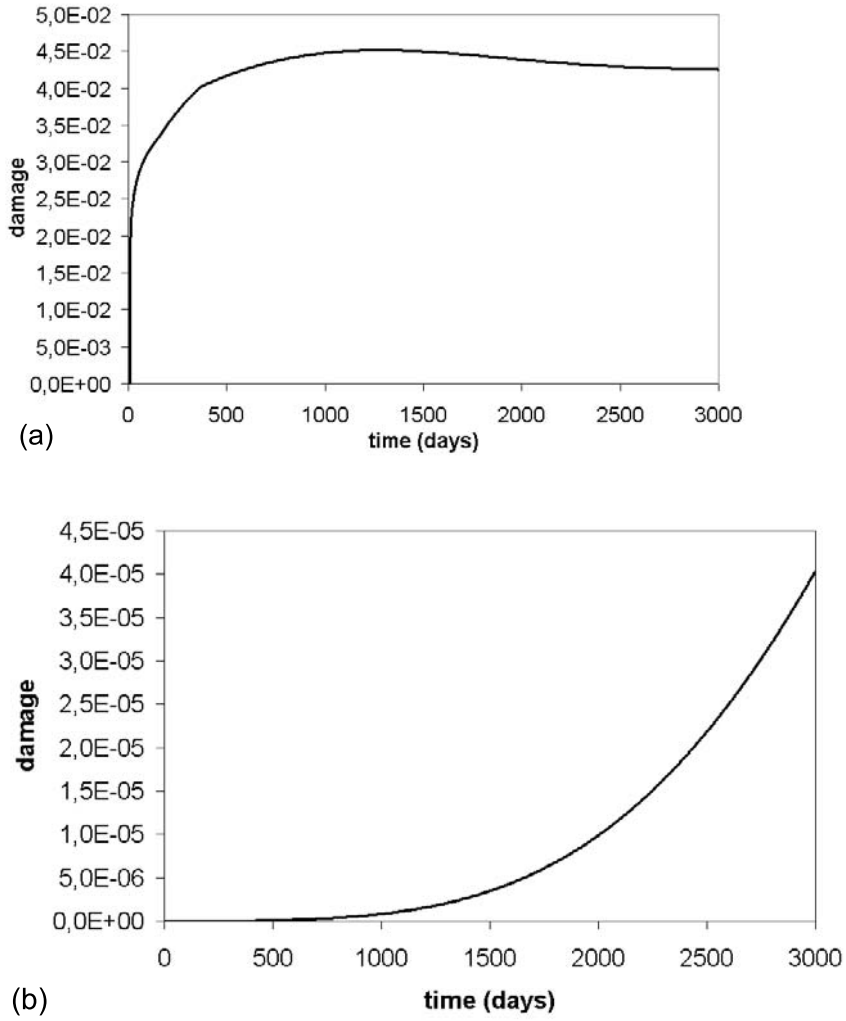

Figure 5. Microdamage accumulation under high overload in bones with different initial densities: (a)$\rho_0 = 2.05$ and (b)$\rho_0 = 1.0\, g/cm^3$ [7]

of movement [62, 63], or non-union is produced if this movement is very large.

Although there is experimental evidence that the regenerative events that occur during fracture healing are influenced by the mechanical conditions [62] [63], it is very difficult to quantify experimentally at the tissue level how the local mechanical stimulus is related to cell expression and therefore to tissue formation, remodelling and growth. This fact motivated that some researchers started proposing different phenomenological rules [64, 65, 66]. These theories and new ones have been now tested by means of computational models that, although simplifications of the reality, are useful for different purposes. Next, a review of the most interesting computer-based models is presented.

4.1 State of the Art of Computational Models on Bone Fracture Healing

Most computational models that have been developed to simulate bone fracture healing are based on finite element analyses. They can be divided into three categories: those that, with a known configuration of the callus determined histologically, study the level of strain

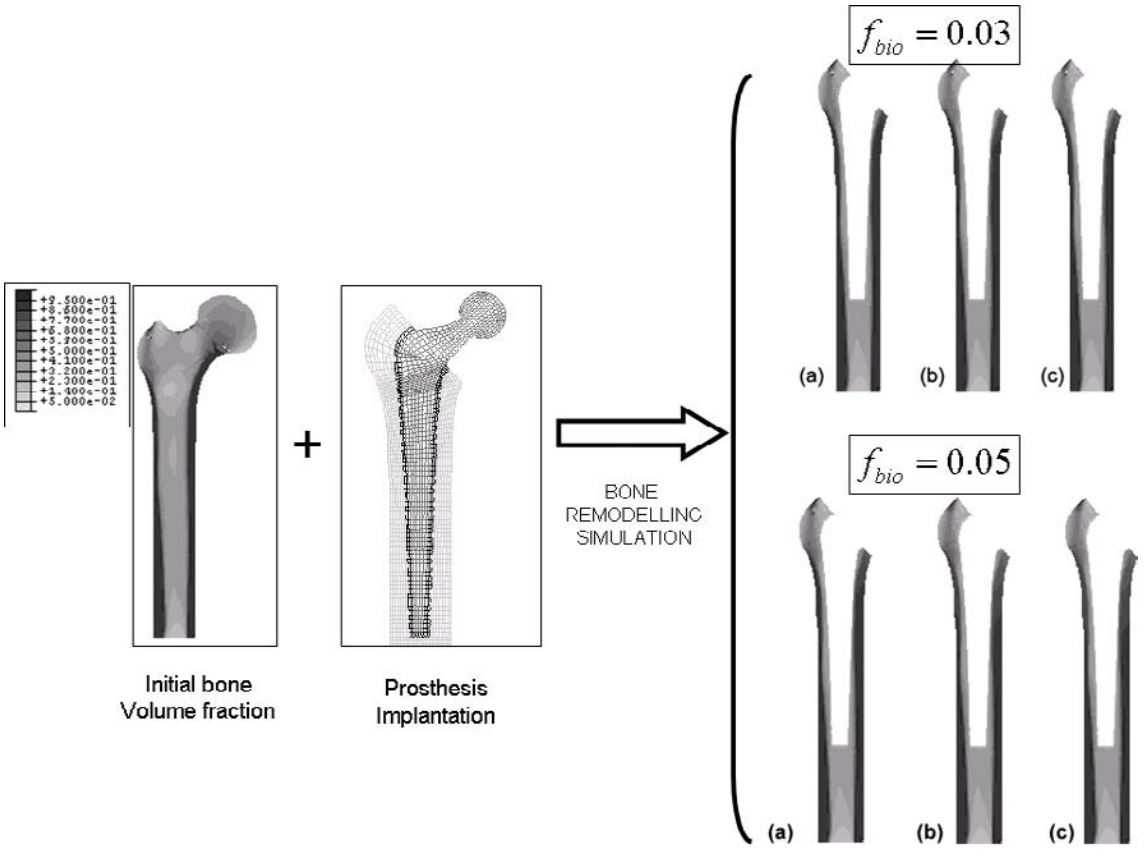

Figure 6. Description of the numerical simulation performed on a 2D model of a femur. After implantation the evolution of the bone volume fraction predicted by the model for different biological factors and for different periods of time is shown: (a) 330, (b) 660 and (c) 990 days

or stress produced in the different tissues [67, 68, 69]; those that study the process of tissue differentiation [70, 71, 72, 73, 74]; and finally models that try to simulate differentiation and callus growth in a coupled way [75, 76, 77].

Carter *et al.* [68, 67] used finite elements to show that the patterns of tissue differentiation observed in fracture healing can be predicted from fundamental mechanobiological rules. And thus they proposed a tissue differentiation theory, which correlates new tissue formation with the local stress/strain history determined computationally. They suggested several differentiation rules that are graphically summarized in Figure 7. In this figure there are two lines that separate the different tissue regions. To the left of the pressure line, the tissue supports a high hydrostatic pressure which serves as stimulus for the production of cartilaginous matrix; to the right, the hydrostatic pressure is very low, causing the production of bone matrix. There is a limit from which this tissue does not differentiate; this is limited by the boundary line of the right. When the tissue is subjected to high tensile strains (above the tension line) fibrous matrix is produced with cartilage or bone, depending on the hydrostatic pressure level.

In a similar way Claes *et al.* [69] proposed a quantitative tissue differentiation theory that relates the tissue strain and the hydrostatic pressure with the new tissue regenerated in the fracture healing process (see Figure 8). They predicted these regulatory laws studying three different healing stages (see Figure 9) quantified experimentally in a sheep model.

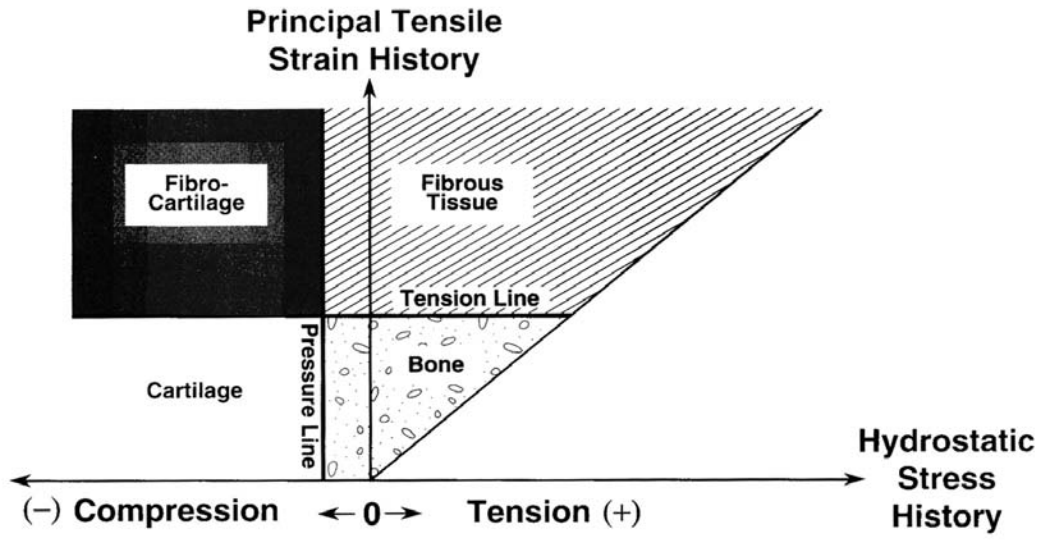

Figure 7. Relationship between mechanical stimulus and tissue differentiation (From [68] with permission)

Kuiper *et al.* [78, 79, 75] developed a differentiation tissue theory using the tissue shear strain and fluid shear stress as the mechanical stimuli regulating tissue differentiation and the strain energy as the mechanical stimulus regulating bone resorption. They used an axisymmetric biphasic model of finite elements of a fracture and applied movements on the cortical bone in an attempt to predict typical healing patterns including callus growth. The results showed that larger movements increased callus size and delayed bone healing.

Lacroix *et al.* [80, 72] predicted successfully, by means of FEA, many different bone fracture healing patterns in the case of a fixed callus. For this purpose they used the phenomenological differentiation rules proposed by Prendergast *et al.* [70] (see Figure 10) to predict interfacial tissue formation between implant and bone.

Ament and Hofer [76] proposed a tissue regulation model based on a set of fuzzy logic rules derived from medical experiments, using the strain energy density as the mechanical stimulus that controls the process of tissue differentiation.

In their first work, Bailon-Plaza and van der Meulen [71] studied the fracture healing process controlled by growth factors with a fixed geometry of the external callus. They used the finite differences method to simulate the sequential tissue regulation and the different cellular events, including haptokinetic and haptotactic mesenchymal cell migration depending on the matrix densities, space-limited cell proliferation as well as environment-dependent cell differentiation, growth factors and matrix production and resorption. In a posterior work, they included the influences of mechanical factors modulating cell differentiation and ossification.

More recently, Gómez *et al.* [77] developed a continuum mathematical model that simulates the process of tissue regulation and callus growth, taking into account different cellular events (i.e., mesenchymal cell migration; mesenchymal cell, chondrocyte, fibroblast and osteoblast proliferation, differentiation and dead), and matrix synthesis, degradation, damage, calcification and remodelling over time. This model is also a particularization of the general formulation proposed in the first part of this paper. It will be used as an example of application of this formulation.

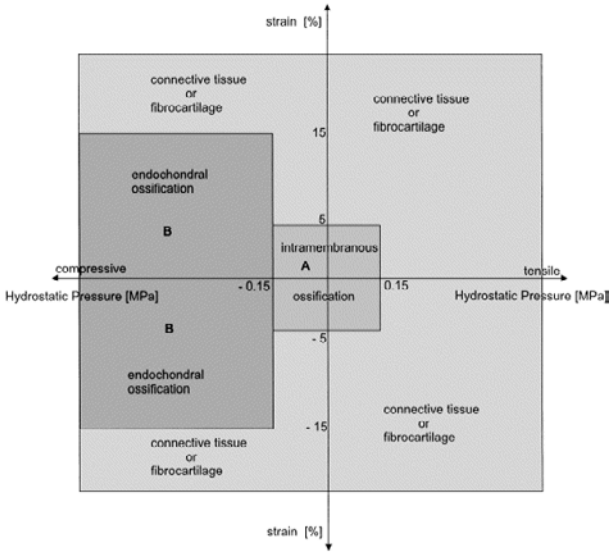

Figure 8. Tissue differentiation rules proposed by Claes and Heigele [69]

4.2 Particularization of the General Formulation to Bone Fracture Healing

In order to understand the model proposed by Gómez *et al.* [77] as a particularization of the general framework presented in this work it is necessary to take into account the following global simplifications:

1. We assume that all processes involved in bone fracture healing (tissue growth, differentiation and damage) are guided by a single mechanical stimulus: the second invariant of the deviatoric strain tensor ($\varphi \equiv J_2$).

2. We have simplified the growth law, working on small strains.

3. The cellular-specific Helmholtz free energy is independent of the elastic strain gradient tensor and temperature, so $\Psi_c^j = \hat{\Psi}_c^j(c_0^j)$. This assumption has important implications on the constitutive equations. Actually, in this particular case, cellular stresses become null $\boldsymbol{P}_c^j \boldsymbol{F}^{g^{jT}} = c_0^j \dfrac{\partial \Psi_c^j}{\partial \boldsymbol{F}^{e^j}} = \boldsymbol{0}$. A similar conclusion can be obtained for the entropy η_c^i per unit cell: from (67) $H_c^j = -\dfrac{\partial \Psi_c^j}{\partial \theta} = 0$. In the constitutive equation (72) the gradient of the cellular-specific Helmholtz free energy can be operated as $\boldsymbol{\nabla} \Psi_c^j = \dfrac{\partial \Psi_c^j}{\partial c_0^j} \boldsymbol{\nabla} c_0^j = \mu \boldsymbol{\nabla} c_0^j$, with μ normally known as *cellular electro-chemical potential*. Therefore, considering that $\boldsymbol{V}_c^j = \dfrac{\boldsymbol{F}\boldsymbol{M}_c^j}{c_0^j}$, the constitutive relation (72) is then particularized to:

$$\boldsymbol{M}_c^j = -\boldsymbol{H}_c^j \boldsymbol{\nabla} \Psi_c^j = -\boldsymbol{H}_c^j \mu \boldsymbol{\nabla} c_0^j = -\boldsymbol{D}_c^j \boldsymbol{\nabla} c_0^j \tag{88}$$

being $\boldsymbol{D}_c^j = \boldsymbol{H}_c^j \mu$ the so-called cell diffusion tensor. In this particular case we have considered that $\Psi_c^j = 0$ for all cells, except for stem cells.

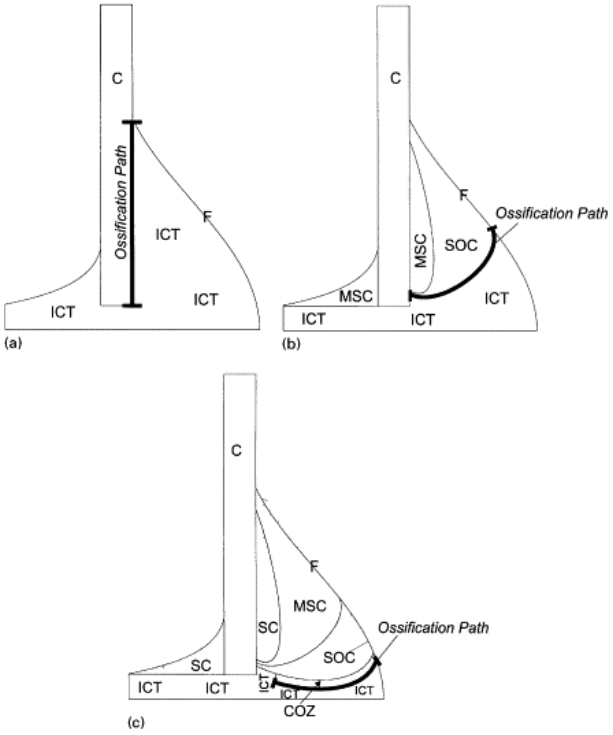

Figure 9. Material properties and ossification paths for the three modelled healing stages: (a) first stage (1 week); (b) second stage (4 weeks); (c) third stage (8 weeks)(From [69] with permission)

4. We consider that the different tissues involved in the healing process can be constituted by: bone (b), cartilage (c), fibrous tissue (f), granulation tissue (g) and debris tissue (d). We consider the different cell types associated respectively with each of these tissues: bone cells (c_b), cartilage cells (c_c), fibroblasts (c_f), mesenchymal stem cells (c_s) and dead cells (c_d). All cells, except dead ones, produce extracellular matrix of the associated tissues. Obviously, debris tissue is not produced by dead cells, but it is a consequence of disruption of healthy tissue, and therefore, this kind of tissue is only considered in the initial conditions of the simulation.

5. All species (except fluid) are assumed to be not diffusive ($\boldsymbol{M}^i = \mathbf{0}$, if $i \neq f$), therefore, we can use the mixture rule to define tissue mechanical properties.

6. As a first approach, we assume that the only tissues with non-negligible mechanical damage are granulation and debris tissues.

Next, cellular balance, mass balance and growth equations are particularized for this specific example.

4.2.1 Balance of cells

The evolution of each kind of cell considered in the model is determined through Eq.(22). Next we particularize the terms Π_c^i and $\boldsymbol{\nabla} \cdot \boldsymbol{M}_c^i$ for each cell type. The net production of cells is controlled by terms A_{pr}^i and A_j^i in Eq.(26).

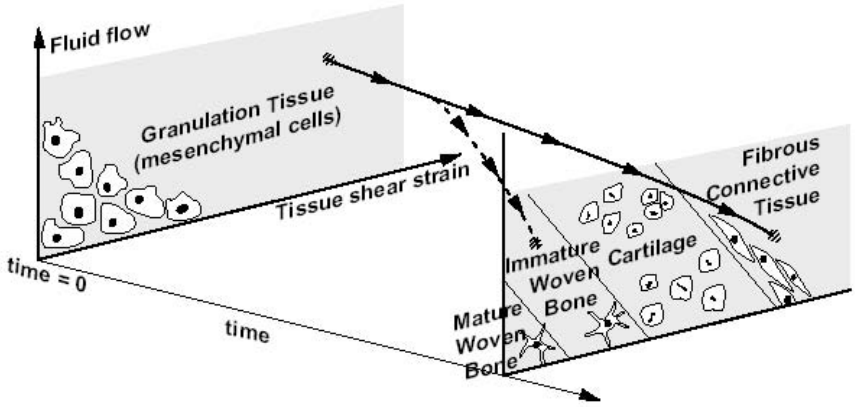

Figure 10. Tissue differentiation law based on mechanical strain and fluid flow (From [72] with permission)

Mesenchymal stem cells

We assume that mesenchymal stem cell proliferation is regulated by the mechanical stimulus; so, we proposed:

$$A^s_{pr} = \frac{\alpha_{pr} \cdot \varphi(\mathbf{x}, t)}{\varphi(\mathbf{x}, t) + \varphi_{pr}} \tag{89}$$

where A^s_{pr} is the stem cell production per unit time and unit cell, φ the mechanical stimulus and α_{pr}, φ_{pr} model constants (see [77]).

Mesenchymal stem cells only appear as consequence of proliferation, they cannot differentiate from other cells, so

$$A^s_b = A^s_c = A^s_f = 0 \tag{90}$$

However, mesenchymal stem cells can differentiate into other cells: bone cells (intramembranous ossification), cartilage cells (chondrogenesis) and fibroblasts. Some authors [81] suggest, based on their experimental works, that tissue differentiation, and consequently, mesenchymal cell differentiation, are mechanobiologically dependent. Using this idea we propose a set of mechanoregulated rules by means of functions $A^b_s(\varphi, t), A^c_s(\varphi, t), A^f_s(\varphi, t)$ and $A^d_s(\varphi, t)$ that control the process of stem cell differentiation into each specialized cell as a function of the mechanical stimulus φ and time t, and that will be defined in the next sections.

As the flux of cells is defined through the constitutive equation (67) and particularized to (88), $\boldsymbol{\nabla} \cdot \boldsymbol{M}^s_c$ is

$$\boldsymbol{\nabla} \cdot \boldsymbol{M}^s_c = -\boldsymbol{\nabla} \cdot (\boldsymbol{D} \boldsymbol{\nabla} c^s_0) = -c^s_0 \boldsymbol{\nabla} \cdot \boldsymbol{D} - \boldsymbol{D} \boldsymbol{\nabla}^2 c^s_0 \tag{91}$$

where $\boldsymbol{D}$ is the diffusion matrix that is assumed to be isotropic $\boldsymbol{D} = D\boldsymbol{1}$. We assume that stem cells can move easily in a non-disrupted tissue, but if disrupted is not able to support their movement. Therefore we have defined this diffusion coefficient D as dependent on the damage level of the granulation tissue d^g_0:

$$D(d^g_0) = D_0 \cdot \frac{1 - d^g_0}{d^g_0 + w} \tag{92}$$

with w a parameter of the model [77].

Although $\boldsymbol{D}$ is not completely uniform, as a first approach, we assume that its divergence is negligible $c_0^s \boldsymbol{\nabla} \cdot \boldsymbol{D} \simeq 0$ in comparison with the rest of terms. Therefore the evolution of the mesenchymal stem cells can be finally written as:

$$\frac{\partial c_0^s}{\partial t} = c_0^s [A_{pr}^s - A_s^b - A_s^c - A_s^f - A_s^d] - \boldsymbol{D} \boldsymbol{\nabla}^2 c_0^s \tag{93}$$

Cartilage cells

We assume that chondrocyte proliferation is negligible when compared to differentiation, therefore:

$$A_{pr}^c = 0 \tag{94}$$

Chondrocytes appear as a consequence of stem cell differentiation, although they can disappear if cartilage develops further to be replaced by bone (endochondral bone formation), a process which also occurs in the growth plate.

On one hand, the functions that define the differentiation into cartilage cells can be expressed as:

$$A_s^c(\varphi, t) = \begin{cases} 1 & if\ \varphi_{bone} < \varphi < \varphi_{cartilage}\ and\ t > t_m^c \\ 0 & other\ cases \end{cases} \tag{95}$$

$$A_b^c(\varphi, t) = A_f^c(\varphi, t_m) = 0 \tag{96}$$

φ_{bone} and $\varphi_{cartilage}$ are stimulus limits in which this type of differentiation progresses and t_m^c a parameter that determines the minimum time that stem cells need to differentiate into cartilage cells, all these values are included in [77].

On the other hand, cartilage cells are considered to differentiate into other cells by means of the following expressions:

$$A_c^s(\varphi, t) = 0 \tag{97}$$

$$A_c^b(\varphi, t) = \begin{cases} h_{source}(\varphi, c_0^b) & if\ \varphi < \varphi_{bone}\ ;\ p_{mi} > p_{mi}^{min}\ and\ c_0^b < c_{0_{min}}^b \\ 1 & if\ \varphi < \varphi_{bone}\ ;\ p_{mi} > p_{mi}^{min}\ and\ c_0^b > c_{0_{min}}^b \\ 0 & other\ cases \end{cases} \tag{98}$$

$$A_c^f(\varphi, t) = A_c^d(\varphi, t_m) = 0 \tag{99}$$

with c_b the bone cell density (number of cells/day.mm^3), φ_{bone} the stimulus that limits intramembranous ossification, p_{mi} the percentage of mineralization of cartilage, and p_{mi}^{min} and $c_{0_{min}}^b$ model constants [77].

$A_c^b(\varphi, t)$ defines the appearance of bone cells through endochondral ossification. This process consists of the invasion of cartilage by blood vessels and consequently by bone cells. Chondrocytes within cartilaginous tissue enlarge and die at the same time, but not before producing enzymes that cause the cartilage matrix to be filled with calcium crystals. Then, growing blood vessels start invasion, bringing osteoblasts and matrix-destroying cells called osteoclasts. At this moment, osteoclasts digest cartilage, while osteoblasts begin to secrete hard extracellular matrix material, continuing until they get trapped becoming new osteocytes. Finally cartilage is completely replaced. Therefore $A_c^b(\varphi, t)$ has to characterize this complex event, that in reality is not a process of chondrocyte differentiation to bone cells alone, but a replacement of one tissue by other. In order not to modify the formulation, we assume that the first differentiation only occurs when bone tissue exists, and there is enough vascularization to ensure vessel invasion. Mathematically we describe this process as the incorporation of a source associated to the Laplacian of bone cells c_0^b, such as:

$$h_{source}(\varphi, c_0^b) = D_b \cdot \frac{(\varphi_{bone} - \varphi)}{2 \cdot \varphi_{bone}} \cdot \boldsymbol{\nabla}^2 c_0^b \frac{1}{c_0^c} \tag{100}$$

with D_b the maximum diffusion coefficient.

Once that first ossification occurs, we assume that enough vascularization exists and therefore direct ossification happens. Moreover, we assume that the chondrocyte flux is null $\boldsymbol{M}_c^c = \boldsymbol{0}$, in comparison with the movement of other cells, such as mesenchymal stem cells.

Therefore the dynamics of chondrocyte population is defined by

$$\frac{\partial c_0^c}{\partial t} = c_0^s A_s^c - c_0^c A_c^b \tag{101}$$

Bone cells

Bone cells can appear through intramembranous or endochondral ossification, as consequence of the differentiation of mesenchymal stem cells or cartilage calcification respectively. Migration and proliferation of osteoblasts is considered negligible in comparison with the increase of osteoblast population due to intramembranous and endochondral ossification. Therefore:

$$A_{pr}^b = 0 \tag{102}$$

$$\boldsymbol{M}_c^b = \boldsymbol{0} \tag{103}$$

We propose that the evolution of bone cell density (c_b) is dependent on the mechanical stimulus φ and time (t) through the corresponding functions:

$$A_s^b(\varphi,t) = \begin{cases} D_b \cdot \boldsymbol{\nabla}^2 c_0^b \frac{1}{c_0^s} & \varphi_{lim} < \varphi < \varphi_{bone}\ ;\ t > t_m^b \ and \ c_0^b < c_{0_{min}}^b \\ 1 & \varphi_{lim} < \varphi < \varphi_{bone}\ ;\ t > t_m^b \ and \ c_0^b > c_{0_{min}}^b \\ 0 & other\ cases \end{cases} \tag{104}$$

$$A_c^b(\varphi,t) = (Equation \quad 98) \tag{105}$$

$$A_f^b(\varphi,t) = 0 \tag{106}$$

with D_b a diffusion coefficient(mm^2/day) and t_m^b the maturation time. With this expression, we assume again that when a sufficient level of vascularization is achieved the bone cell differentiation does not depend on this source term and a direct tissue differentiation is produced. The function that defines the direct differentiation of mesenchymal stem cells into bone cells (intramembranous ossification) has been also chosen in a similar way to the endochondral one, that is, by means of a source term, but in this case independent on the mechanical stimulus φ.

As these bone cells mature, they cannot differentiate into other type of cells, therefore we propose:

$$A_b^s = A_b^c = A_b^f = 0 \tag{107}$$

with these assumptions the complete evolution of bone cells can be written as:

$$\frac{\partial c_0^b}{\partial t} = c_0^s A_s^b + c_0^c A_c^b \tag{108}$$

Fibroblasts

The migration and proliferation of fibroblasts is also considered negligible:

$$A_{pr}^f = 0 \tag{109}$$

$$\boldsymbol{M}_c^f = \boldsymbol{0} \tag{110}$$

Fibroblasts appear as consequence of mesenchymal stem cell differentiation. Then:

$$A_s^f(\varphi,t) = \begin{cases} 1 & \varphi_{fibrous} < \varphi < \varphi_{death} \, and \, t > t_m^f \\ 0 & other \, cases \end{cases} \tag{111}$$

$$A_b^f(\varphi,t) = 0 \tag{112}$$

$$A_c^f(\varphi,t) = 0 \tag{113}$$

being $\varphi_{fibrous}$, φ_{death} the limits corresponding to fibroblast differentiation [77].

We also assume that fibroblasts cannot differentiate into other kind of cells, therefore

$$A_f^s = A_f^c = A_f^b = 0 \tag{114}$$

Under these conditions the evolution of fibroblasts would be:

$$\frac{\partial c_0^f}{\partial t} = c_0^s A_s^f \tag{115}$$

Dead cells

Finally, we have also considered the possibility that cells die under a sufficiently high stimulus. The law proposed for this evolution is then

$$A_s^d(\varphi,t) = \begin{cases} 1 & if \, \varphi > \varphi_{death} \\ 0 & other \, cases \end{cases} \tag{116}$$

4.2.2 Balance of mass

As previously remarked, we have considered two different phases: fluid (fl) and solid. But in the solid we distinguish among different kind of species: granulation tissue (g), cartilage (c), bone (b), fibrous tissue (f) and debris (d).

We assume that the balance of mass expressed in (9) is verified for all of these species with null mass flux

$$\boldsymbol{\nabla} \cdot \boldsymbol{M}^i = 0 \qquad i = g, c, b, f, d \tag{117}$$

The time evolution of the real tissue density $\overline{\rho}_0^i$ is also considered null

$$\frac{\partial \overline{\rho}_0^i}{\partial t} = 0 \qquad i = g, c, b, f, d \tag{118}$$

Sometimes, when the bone fracture site is not sufficiently stabilized, healing may not be successful resulting in a non-union. This process normally occurs at the beginning of the healing process. We assume that this effect is mainly due to the micro-fissuration that occur in the newly recent formed tissues, that is, granulation tissue. Therefore, although all tissue types may be susceptible of being damaged, we assume that only granulation and debris tissues can experience this mechanical degradation during the healing process. The rest of tissues like bone, cartilage and fibrous are specialized tissues that have been created as consequence of a cellular differentiation that requires specific mechanical conditions. If these limitations are not fulfilled tissue differentiation process would not happen, which is previous to the occurrence of damage.

Therefore, we assume that

$$\frac{\partial h_0^i}{\partial t} = 0 \qquad i = c, b, f \tag{119}$$

Volume	Debris Tissue	Bone Tissue	Cartilage	Calcified Cartilage	Fibrous Tissue	Granulation Tissue
Collagen I	0.	0.2848	0.	0.	0.1861	0.018
Collagen II	0.	0.	0.135	0.135	0.	0.
Collagen III	0.018	0.	0.	0.	0.	0.
Ground Substance	0.082	0.0352	0.079	0.079	0.07885	0.082
Mineral	0.	0.43	0.	0.015	0.	0.

Table 1. Composition used for each different tissue type [57]

and

$$f(\varphi) = \varphi - \varphi_{damage} => \begin{cases} \text{if} \quad f < 0 => \frac{\partial h_0^i}{\partial t} = 0 \\ \text{if} \quad f > 0 => \frac{\partial h_0^i}{\partial t} > 0 \end{cases} \qquad i = g, d \tag{120}$$

with this, Eq.(9) is simplified to

$$\frac{\partial \rho_0^i}{\partial t} = \overline{\rho}^i \frac{\partial V_m^i}{\partial t} = \Pi^i \qquad i = c, b, f \tag{121}$$

and

$$\frac{\partial \rho_0^i}{\partial t} = \overline{\rho}^i \frac{\partial V_m^i}{\partial t}(1 - h_0^i) + \overline{\rho}^i V_m^i (-\frac{\partial h_0^i}{\partial t}) = \Pi^i \qquad i = g, d \tag{122}$$

Obviously, this micro-fissuration process causes a mechanical degradation quantified by means of damage variable d_0 as was shown in (19). As a first approach, we have also considered a linear relationship between both variables h_0 and d_0, following expression (84).

We assume that mass generation is always produced, keeping constant the composition of the extracellular matrix (ECM) for each different tissue (see Table 1), so we propose the next expression for each tissue:

$$\begin{aligned} \frac{\Pi^g}{\overline{\rho}^g} &= c_0^s \cdot B_s^g + c_0^c B_c^g + c_0^b B_b^g + c_0^f B_f^g & B_s^g \geq 0; B_c^g, B_b^g, B_f^g \leq 0 \\ \frac{\Pi^c}{\overline{\rho}^c} &= c_0^c \cdot B_c^c + c_0^b B_b^c & B_c^c \geq 0; B_b^c \leq 0 \\ \frac{\Pi^b}{\overline{\rho}^b} &= c_0^b \cdot B_b^b & B_b^b \geq 0 \\ \frac{\Pi^f}{\overline{\rho}^f} &= c_0^f \cdot B_f^f & B_f^f \geq 0 \end{aligned} \tag{123}$$

where B_j^i is the net matrix production of tissue i per cell j and unit time and c_0^i is the cell density i associated to each tissue.

We assume this expression is valid for all tissues except for mature bone, in which the development of bone matrix volume is determined using the internal bone remodelling formulation proposed by Beaupré *et al.* [50, 82]:

$$\frac{\Pi^b}{\overline{\rho}^b} = k_{rem} \cdot \dot{r} \cdot S_v \quad if\ 0 < \varphi < \varphi_{mature} \tag{124}$$

where $\dot{r}$ is the formation/resorption of bone matrix volume per available bone surface per time, S_v is the specific bone surface measured by Martin [58] and k_{rem} is the percentage of

bone surface that is active for remodelling. Although this remodelling law is phenomenological, it allows to consider in a simplified way the influence on healing of bone remodelling. Obviously, more complex bone remodelling theories can be used, even including the actual effect of bone cells by means of packets of BMUs as has been shown in the previous example.

We also consider that damaged tissue can be repaired when the stimulus level is low enough. In this case, we assume that stem cells can produce new matrix repairing the disrupted matrix in a proportional way similar to that proposed previously in (21):

$$\frac{\partial d_0^g}{\partial t} = -\frac{\partial V_m^g}{\partial t}\frac{d_0^g}{V_m^g} \qquad \text{or equivalently} \qquad \frac{\partial h_0^g}{\partial t} = -\frac{\partial V_m^g}{\partial t}\frac{h_0^g}{V_m^g} \tag{125}$$

Due to the linear relation between h_0 and d_0 we have used the latter as independent variable, without the need of evaluating h_0 and therefore not establishing the value of k, which is not actually known.

4.2.3 Kinematics of growth

As a first approach we work under the theory of small deformations. Therefore, if the deformation gradient tensor is written in terms of the displacement gradient tensor $\boldsymbol{L}$ as $\boldsymbol{F} = \mathbf{1} + \boldsymbol{L}$, then the product $\boldsymbol{F}^g\boldsymbol{F}^e$ can be expanded to

$$\boldsymbol{F} = \boldsymbol{F}^g\boldsymbol{F}^e = (\mathbf{1} + \boldsymbol{L}^g)(\mathbf{1} + \boldsymbol{L}^e) = \mathbf{1} + \boldsymbol{L}^g + \boldsymbol{L}^e + \boldsymbol{L}^g\boldsymbol{L}^e \tag{126}$$

that under small deformations simplifies to

$$\boldsymbol{F} = \boldsymbol{F}^g\boldsymbol{F}^e \simeq \mathbf{1} + \boldsymbol{L}^g + \boldsymbol{L}^e \tag{127}$$

We assume that callus growth is mainly due to two different processes that are essentially isotropic and that occur in different tissues: mesenchymal cell proliferation (granulation tissue) and endochondral ossification in cartilage. Therefore we propose the following expressions:

$$\begin{aligned} \boldsymbol{L}^{g^g} &= f_{pr}^v(c_s, \varphi)\boldsymbol{1} \\ \boldsymbol{L}^{g^c} &= g_{end}^v(\varphi, t)\boldsymbol{1} \end{aligned} \tag{128}$$

where $g_{end}^v(\varphi, t)$ controls the rate of callus growth due to endochondral ossification and $f_{pr}^v(c_s, \varphi)$ defines the rate of callus growth due to proliferation.

It is assumed that the concentration of mesenchymal cells can proliferate from zero to a maximum or saturation cell density. When the saturation concentration of stem cells is reached the only way cells can proliferate is increasing the callus size at a constant level of cell concentration:

$$f_{pr}^v = \begin{cases} 0 & if c_0^s < c_{max}^s \\ \frac{c_0^s}{c_{max}^s} & if c_0^s > c_{max}^s \end{cases} \tag{129}$$

where $c_0^s(\mathbf{x}, t)$ is the stem cell density (number of stem cells/mm^3) and c_{max}^0 is the saturation stem cell density (number of stem cells/mm^3).

During endochondral ossification cartilage cells increase their volume up to ten times their original volume [83], extracellular matrix cartilage calcifies and is later replaced by bone. The number of cartilage cells is almost constant during this process [84], which allows to define growth as:

$$g_{end}^v(\varphi, t) = \begin{cases} \frac{\varphi - \varphi_{calcified}}{\varphi_{bone} - \varphi_{calcified}} \cdot \frac{k_{hyper}}{c_0^c} & if\ (\varphi < \varphi_{calcified})\ and\ (c_0^c < c_{min}^c) \\ 0 & in\ other\ cases \end{cases} \tag{130}$$

with $\varphi_{calcified}$, k_{hyper} and c^c_{min} constants of the model.

It is assumed that the change of chondrocyte density is produced in order to get an equilibrium value (c^c_{min}). When this value is reached the volume growth becomes zero. Moreover, with this growth law $\boldsymbol{L}^g$ is compatible.

4.2.4 Material behaviour

All tissues are assumed to be biphasic and isotropic. The material properties of the different tissues, except for mature bone, are determined using a mixture rule, similar to other authors [85, 72]. The modulus of elasticity E and the Poisson´s ratio ν are determined from the proportion of each component p_x (the subscript x denotes the specific component indicated in Table 1):

$$\begin{cases} E(MPa) = 2000p_{mi} + 430p_{cI} + 200p_{cII} + 100p_{cIII} + 0.7p_{gs} \\ \nu = 0.33p_{mi} + 0.48p_{coll} + 0.49p_{gs} \end{cases} \tag{131}$$

Properties of mature bone are determined as a function of the apparent density [86]:

$$\begin{cases} E = 2014 \cdot \rho^{2.5}, \nu = 0.2 & if\ \rho \leq 1.2g/cc. \\ E = 1763 \cdot \rho^{3.2}, \nu = 0.32 & if\ \rho \geq 1.2g/cc. \end{cases} \tag{132}$$

Permeability is also different for each type of tissue. In soft tissues, permeability was computed according to its composition and porosity, following the model proposed by Levick [87]. However, for hard tissues, we assumed constant permeability distinguishing between cortical and trabecular bone, and calcified cartilage, with respective values of 7x10^{-15} mm^2, 7x10^{-11} mm^2 and 3.5x10^{-12} mm^2.

Moreover we have considered the possibility of loss of stiffness as consequence of tissue disruption in granulation tissue. As a result of this disruption the elastic modulus of the granulation tissue is reduced as follows:

$$E^g_{new} = E^g_0(1 - d^g_0) \tag{133}$$

where E_0 is the elastic modulus of the intact granulation tissue.

4.2.5 Numerical example

This formulation has been implemented in a Finite Element commercial code in combination with an automatic mesh generation program [88]. An updated Lagrangian approach was used; therefore a continuous update of the mesh is required because fracture callus progressively grows during healing, modifying its shape and geometry. All independent variables, cell concentration c^i_0 for each cell type i and variables associated to extracellular matrix were stored as nodal values. The callus shape was defined by the position of the nodes. Each loading increment was divided in three different analysis steps (see Figure 11). In the first step, the mechanical stimulus was determined using a biphasic analysis. Next, a diffusion analysis was performed to simulate the migration of stem cells and the advance of the ossification front. With the mechanical stimulus determined at each node, growth is calculated due to stem cell proliferation and chondrocyte hypertrophy, and thus, a "thermoelastic" analysis step was performed to determine the new position of the nodes and the new callus geometry. With this idea, the local cell density (mesenchymal stem cells or chondrocytes) was used as thermal expansion coefficient, while the values of the cellular proliferation (Eq.(129)) and the chondrocyte growth function (130) were used as temperature rise. Nodal positions were updated using the displacements calculated in the third step, and the new positions were used to define a new callus geometry. Finally, all variables of the model were updated. After each loading increment, a new 3D mesh of tetrahedral

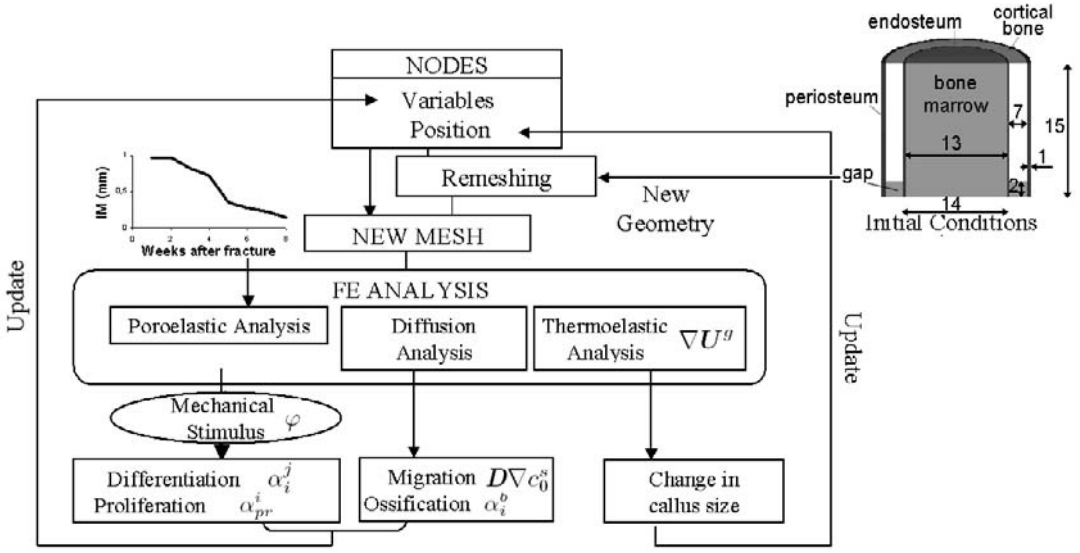

Figure 11. Scheme of the numerical implementation

Volume Collagen I	Gap 0.	Periosteum 0.018	Endosteum 0.02	Medular channel 0.	Cortical Bone 0.2706
Collagen II	0.	0.	0.	0.	0.
Collagen II	0.	0.	0.	0.	0.
Collagen III	0.018	0.0	0.	0.018	0.
Ground Substance	0.082	0.082	0.08	0.082	0.0334
Mineral	0.	0.	0.	0.	0.4085
Water	0.9	0.9	0.9	0.9	0.2375
Pore volume	0.	0.	0.	0.	0.0
Pore volume	0.	0.	0.	0.	0.05

Table 2. Initial composition in % volume used for the simulation

elements was automatically generated from the position of nodes using the Detri mesh generator [88].

In order to study the potential of this approach, we have analyzed the 3D evolution of the periosteal callus of a simplified human tibia fracture (see Figure 12) that has been simulated as a cylinder with symmetric conditions in the line through the fracture gap. The healing fracture has been studied for a simple loading case corresponding to an axial interfragmentary displacement. Obviously the history of this displacement changes with time depending on the stiffness of the fixator used to treat the fracture and the reparative evolution of the callus. In this simple example, we have used a loading history measured experimentally [89] (see Figure 11) in a fracture of this kind. All the model parameters have been taken from a previous work of the same authors [77]. As initial conditions for cells we assumed that the gap and medullar channel were empty of cells, the periosteum full of undifferentiated mesenchymal cells and there existed a small layer of osteoblasts between cortical bone and periosteum. Regarding material initial conditions, we considered the components distribution distinguishing among different spatial regions presented in Table 2.

Figure 12 shows the first 8 weeks of temporal evolution for stem cell, bone cell and chondrocyte density, according to the mechanical stimulus proposed. Initially, mesenchymal cells

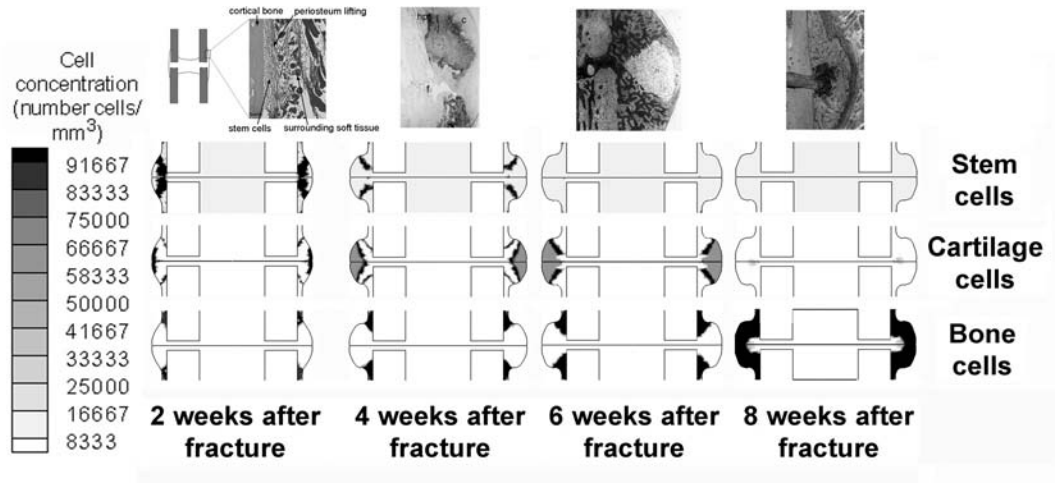

Figure 12. Cellular distributions at different times of the healing process: numerical results and histological sections (histologies taken from van der Meulen, Cornell University, NY; Sarmiento and Russell http://www.hwbf.org/ota/bfc/index.htm, 2002; [62])

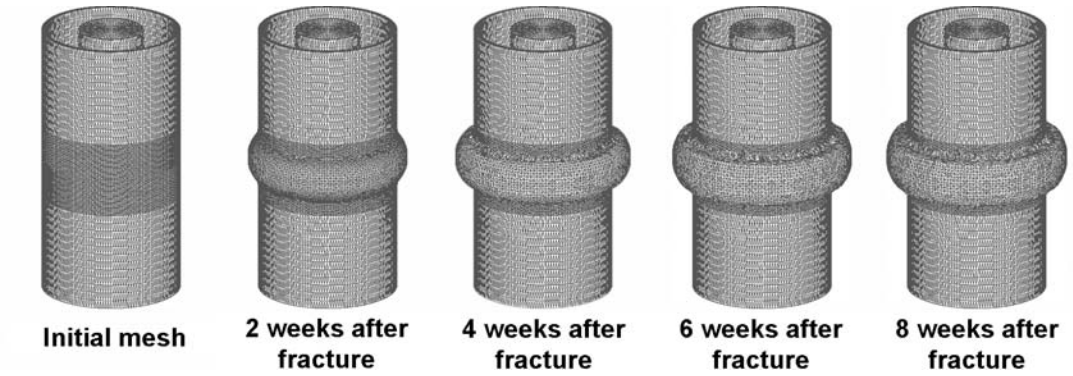

Figure 13. Meshes showing the evolution of the callus

proliferate quickly in the callus site, leading to the corresponding callus growth. First, calcification in humans occurs 7 days after injury in the inner periosteum as intramembranous ossification and the differentiation of stem cells into osteoblasts is also shown at this time. By day 14, chondrogenesis (stem cell differentiation into chondrocytes) is produced quickly in the callus, occupying most of the callus.

Endochondral ossification in humans requires from 4 to 16 weeks [90]. In the model this process begins in the 4th week and requires about 8 weeks (12). The rate of this event depends directly on the stability of the fracture and additional factors, such as physiological or metabolical. In this case, the process is controlled by the interfragmentary movement applied, which has been measured for the evolution of a successful fracture healing [89]). And thus, in our simulation, after 8 weeks we can see how the callus is fully formed and mineralized. Chondrocyte population has disappeared and bone cells occupy the larger part of the callus.

Therefore this model is able to simulate the different cellular events that are normally involved in fracture healing and the progressive evolution of the callus (see Figure 13).

5 CONCLUDING REMARKS

We have presented in this paper a general constitutive theory for growth, differentiation, remodelling and damage of living tissues. The theory is formulated using as main continuum variables the ECM matrix density of each specie and the cell population density of each cell. The balance laws are determined and the constitutive relations deduced.

The continuum approach analyzes the evolution of ECM for different tissues and cell populations. The model includes biophysical facts like: ECM deposition for each specie due to cells, ECM degradation caused by mechanical stimulus, and cell activities (proliferation, differentiation and migration) regulated by mechanical influences. This model is able to describe the development of biological tissues, taking into account the complex behavior of cell-ECM interactions, mechanical influences and time.

Two particularizations have been developed to show its potential applicability. First, the simulation of bone remodelling corresponds to a particular case of this theory, in which only the influence of damage in the bone remodelling process is analyzed, not considering growth nor differentiation. This formulation has been presented and numerically implemented in a previous work developed by García-Aznar *et al.* [7]. In the second example, we used the general framework to model a more complex process, such as bone fracture healing, where growth, differentiation and damage act on the tissue. This has also been implemented numerically in a previous work [77], illustrating a qualitative reasonable prediction of the resulting cell and tissue distribution patterns.

In spite of some simplifications in both examples, they have been able to predict several biophysical features in qualitative agreement with well-known experimental or clinical results.

Although the numerical implementations here shown present some simplifications (small deformations, no residual stresses, null cell-matrix interaction, etc.) the global formulation proposed is sufficiently general to be used in other biomechanical applications, such as limb lengthening, tendons and vessels growth and remodelling, and others.

Nevertheless and although this approach is completely general, some aspects have not been considered. For example, in the case of stem cell motion we have only analyzed the Fick's law, whereas the model proposed by Oster *et al.*. [17] includes the interaction with other cells beyond their nearest neighbors via an additional biharmonic diffusion term and that cells tend to move from less to more adhesive regions of their substrata (haptotaxis term). However the inclusion of this effect would be easy. The model here presented only consider mechanical influences, although other mathematical models of fracture healing and development [71, 91] have considered the regulatory effects of growth factors and morphogens. Nevertheless, we have to keep in mind that both effects mainly contribute to the way of mechanical signals are translated into cell activities (gene expression, differentiation, metabolism and motility). In fact, when a tissue is deformed induces extracellular matrix deformation and interstitial fluid flow; these cause mechanical effects on the cells. At the same time, soluble biologic factors, such as, growth factors, hormones and cytokines, in the interstitial fluid or attached to the matrix initiate intracellular processes that influence on how cells sense and respond under this mechanical environment.

ACKNOWLEDGEMENT

Research partially supported by the Spanish Ministry of Science and Technology through the research project DPI2004-07410-C03-01.

APPENDIX I

For saturated biphasic tissues with solid (s) and fluid (f) phases, the saturation condition becomes

$$v_m^s + v_m^f = 1 \tag{134}$$

If we operate in the balance of mass of both solid and fluid in the current configuration, replacing $\boldsymbol{v}$ by $\boldsymbol{v}^s$ and redefining $\boldsymbol{v}^f$ as the total fluid velocity, that is, substituting in all the previous formulae $\boldsymbol{v}^f$ by $\boldsymbol{v}^f - \boldsymbol{v}^s$, and particularizing for $h^s = 0$, $\pi^s = 0$, $\bar{\rho}^s = constant$ and $\bar{\rho}^f = constant$, we obtain from (10) the following equations:

$$\bar{\rho}^s \frac{dv_m^s}{dt} + \rho^s \boldsymbol{\nabla} \cdot \boldsymbol{v}^s = \bar{\rho}^s \frac{dv_m^s}{dt} + \bar{\rho}^s v_m^s \boldsymbol{\nabla} \cdot \boldsymbol{v}^s = 0 \tag{135}$$

$$\bar{\rho}^f \frac{dv_m^f}{dt} + \bar{\rho}^f v_m^f \boldsymbol{\nabla} \cdot \boldsymbol{v}^s = -\boldsymbol{\nabla} \cdot \boldsymbol{m}^f \tag{136}$$

As $\boldsymbol{m}^f = -\rho^f(\boldsymbol{v}^s - \boldsymbol{v}^f) = -\bar{\rho}^f v_m^f(\boldsymbol{v}^s - \boldsymbol{v}^f)$ then previous expressions can be written as:

$$\frac{dv_m^s}{dt} = -v_m^s \boldsymbol{\nabla} \cdot \boldsymbol{v}^s \tag{137}$$

$$\frac{dv_m^f}{dt} = -v_m^f \boldsymbol{\nabla} \cdot \boldsymbol{v}^s + \boldsymbol{\nabla} \cdot (v_m^f \boldsymbol{v}^s - v_m^f \boldsymbol{v}^f) \tag{138}$$

If we combine these balance equations with the saturation condition (134), we obtain:

$$-(v_m^s + v_m^f)\boldsymbol{\nabla} \cdot \boldsymbol{v}^s + \boldsymbol{\nabla} \cdot [(1 - v_m^s)\boldsymbol{v}^s - v_m^f \boldsymbol{v}^f] \tag{139}$$

and operating we finally obtain the standard continuity equation for biphasic systems:

$$\boldsymbol{\nabla} \cdot (v_m^s \boldsymbol{v}^s + v_m^f \boldsymbol{v}^f) = 0 \tag{140}$$

As the fluid is considered incompressible, it means that its mass-specific Helmhotz free energy does not depend on the strain. In this case it is usual to modify the definition of the mass-specific Helmholtz free energy in the current configuration adding the saturation condition (134) by means of a Lagrange multiplier p:

$$\Sigma_i \rho^i \psi^i = \rho^s \overline{\psi}^s + p(v_m^s + v_m^f - 1) \tag{141}$$

Using this condition in the Clausius-Duhem inequality expressed in the current configuration, we get:

$$\begin{aligned} &\rho^s [J^{-1}(\frac{\partial \overline{\psi}^s}{\partial \boldsymbol{F}} \cdot \boldsymbol{F}^T) : \boldsymbol{\nabla} \boldsymbol{v}^{\boldsymbol{s}} + \frac{\partial \overline{\psi}^s}{\partial \theta} \dot{\theta} + \eta^s \dot{\theta}] + (v_m^s + v_m^f - 1)\dot{p} + p(\dot{v}_m^s + \dot{v}_m^f) - \\ &-\boldsymbol{\sigma}^{\boldsymbol{s}} : \boldsymbol{\nabla} \boldsymbol{v}^s - \boldsymbol{\sigma}^{\boldsymbol{f}} : \boldsymbol{\nabla} \boldsymbol{v}^f + \rho^s \boldsymbol{l}^s \cdot \boldsymbol{v}^s + \rho^f \boldsymbol{l}^f \cdot \boldsymbol{v}^f + \\ &+\pi^s (\overline{\psi}^s + \theta \eta^s + \frac{1}{2} \|\boldsymbol{v}^{\boldsymbol{s}}\|^2)] \leq 0 \end{aligned} \tag{142}$$

Using the balance of mass, replacing again $\boldsymbol{v}$ by $\boldsymbol{v}^s$ and $\boldsymbol{v}^f$ by $\boldsymbol{v}^f - \boldsymbol{v}^s$, and using the definition of the fluid flux $\boldsymbol{m}^f = \rho^f(\boldsymbol{v}^f - \boldsymbol{v}^s)$ we obtain:

$$\begin{aligned}
&\rho^s[J^{-1}(\frac{\partial\overline{\psi}^s}{\partial\boldsymbol{F}}\cdot\boldsymbol{F}^T):\boldsymbol{\nabla}\boldsymbol{v^s}+\frac{\partial\overline{\psi}^s}{\partial\theta}\dot{\theta}+\eta^s\dot{\theta}]+(v_m^s+v_m^f-1)\dot{p}+\\
&+p[\frac{\pi^s}{\bar{\rho}^s(1-d^s)}-v_m^s\boldsymbol{\nabla}\cdot\boldsymbol{v}^s+\frac{\dot{d}^s}{1-d^s}-\frac{d\bar{\rho}^s}{dt}\frac{1}{\bar{\rho}^s}]+\\
&+p[-v_m^f\boldsymbol{\nabla}\cdot\boldsymbol{v}^s-\boldsymbol{\nabla}\cdot(v_m^f(\boldsymbol{v}^f-\boldsymbol{v}^s))]-\\
&-\boldsymbol{\sigma^s}:\boldsymbol{\nabla}\boldsymbol{v}^s-\boldsymbol{\sigma^f}:\boldsymbol{\nabla}\boldsymbol{v}^f+\rho^s\boldsymbol{l}^s\cdot\boldsymbol{v}^s+\rho^f\boldsymbol{l}^f\cdot\boldsymbol{v}^f+\\
&+\pi^s(\overline{\psi}^s+\theta\eta^s+\frac{1}{2}\|\boldsymbol{v^s}\|^2)]\leq 0
\end{aligned}\tag{143}$$

Collecting terms we get:

$$\begin{aligned}
&\rho^s[J^{-1}(\frac{\partial\overline{\psi}^s}{\partial\boldsymbol{F}}\cdot\boldsymbol{F}^T)-pv_m^s\mathbf{1}-\boldsymbol{\sigma^s}]:\boldsymbol{\nabla}\boldsymbol{v^s}+\rho^s(\frac{\partial\overline{\psi}^s}{\partial\theta}+\eta^s)\dot{\theta}+(v_m^s+v_m^f-1)\dot{p}+\\
&+p[\frac{\pi^s}{\bar{\rho}^s(1-d^s)}+\frac{\dot{d}^s}{1-d^s}-\frac{d\bar{\rho}^s}{dt}\frac{1}{\bar{\rho}^s}]-\\
&-(pv_m^f\mathbf{1}+\boldsymbol{\sigma^f}):\boldsymbol{\nabla}\boldsymbol{v}^f+\\
&+(-p\boldsymbol{\nabla}v_m^f+\rho^f\boldsymbol{l}^f)\cdot\boldsymbol{v}^f+(-p\boldsymbol{\nabla}v_m^s+\rho^s\boldsymbol{l}^s)\cdot\boldsymbol{v}^s+\\
&+\pi^s(\overline{\psi}^s+\theta\eta^s+\frac{1}{2}\|\boldsymbol{v^s}\|^2)]\leq 0
\end{aligned}\tag{144}$$

In order to verify this inequality we have to fulfill:

$$\begin{aligned}
\boldsymbol{\sigma^s} &= J^{-1}(\frac{\partial\overline{\psi}^s}{\partial\boldsymbol{F}}\cdot\boldsymbol{F}^T)-pv_m^s\mathbf{1}\\
\boldsymbol{\sigma^f} &= -pv_m^f\mathbf{1}\\
\eta^s &= -\frac{\partial\overline{\psi}^s}{\partial\theta}\\
v_m^s+v_m^f-1 &= 0\\
(-p\boldsymbol{\nabla}v_m^f+\rho^f\boldsymbol{l}^f)\cdot\boldsymbol{v}^f &\leq 0\\
(-p\boldsymbol{\nabla}v_m^s+\rho^s\boldsymbol{l}^s)\cdot\boldsymbol{v}^s &\leq 0
\end{aligned}\tag{145}$$

We can also express these equations in the initial configuration as:

$$\begin{aligned}
(\boldsymbol{P}\boldsymbol{F}^T)^s &= \frac{\partial\overline{\Psi}^s}{\partial\boldsymbol{F}}\cdot\boldsymbol{F}^T-pV_m^s\mathbf{1}\\
(\boldsymbol{P}\boldsymbol{F}^T)^f &= -pV_m^f\mathbf{1}\\
H^s &= -\frac{\partial\overline{\Psi}^s}{\partial\Theta}\\
V_m^s+V_m^f-1 &= 0\\
(-p\boldsymbol{\nabla}V_m^f+\rho_0^f\boldsymbol{F}\boldsymbol{L}^f)\cdot\boldsymbol{V}^f &\leq 0\\
(-p\boldsymbol{\nabla}V_m^s+\rho^s\boldsymbol{F}\boldsymbol{L}^s)\cdot\boldsymbol{V}^s &\leq 0
\end{aligned}\tag{146}$$

REFERENCES

1 D'Arcy Wentworth Thompson (1997). *On growth and form*. Cambridge University Press, Cambridge.

2 S.C. Cowin (2004). Tissue growth and remodeling. *Annu. Rev. Biomed. Eng.*, **6**, 77–107.

3 D.R. Carter and G.S. Beaupre (2001). *Skeletal Function and Form*. Cambridge University Press.

4 Marjolein C.H. van der Meulen and Rik Huiskes (2002). Why mechanobiology? A survey article. . *J. of Biomechanics*, **35**, 401–414.

5 R.T. Hart (2001). *Bone modeling and remodeling: theories and computation*. Chapter 31, pp. 31.1–31.42. Bone Mechanics Handbook, 2nd Ed. CRC Press.

6 H.E. Petermann, T.J. Reiter and F.G. Rammerstorfer (1997). Computational simulation of internal bone remodeling. *Archives of Computational Methods in Engineering*, **4**(4), 295–323.

7 J.M. García-Aznar, T. Rueberg and M. Doblaré. A bone remodelling model coupling microdamage growth and repairing by 3D BMU-activity. *Biomech Model Mechanobiol*, In press.

8 R. Skalak, G. Dasgupta, M. Moss, E. Otten, P. Dullemeijer and H. Vilmann (1982). Analytical description of growth. *J. Theor. Biol.*, **94**, 555–577.

9 J.D. Humphrey (1995). Mechanics of the arterial wall: review and directions. *Critic Rev Biomed Engng*, **23**, 1–62.

10 L.A. Taber (1995). Biomechanics of growth, remodelling and morphogenesis. *Appl. Mech. Rev.*, **48**(8), 487–545.

11 M. Doblaré, J.M. García and M.J. Gómez (2004). Modelling bone tissue fracture and healing: a review. *Engineering Fracture Mechanics*, **71** (13-14), 1809–1840.

12 H. Isaksson, W. Wilson, C.C. van Donkelaar, R. Huiskes and K. Ito. Comparison of biophysical stimuli for mechano-regulation of tissue differentiation during fracture healing. *J. Biomech*, in press.

13 V.A. Lubarda, A. Hoger (2002). On the mechanics of solids with a growing mass. *Int. J. Solids Struct.*, **39**, 4627–4664.

14 E. Kuhl and P. Steinmann (2003). Theory and numerics of geometrically non-linear open system mechanics. *Int. J. Numer. Metho. Engng.*, **58**.

15 E. Kuhl and P. Steinmann (2004). Computational modeling of healing: an application of the material force method. *Biomech. Model. Mechanobiol.*, **2** (4).

16 K. Garikipati, E.M. Arruda, K. Grosh, H. Narayanan and S. Calve (2004). A continuum treatment of growth in biological tissue: the coupling of mass transport and mechanics. *Journal of the Mechanics and Physics of Solids*, **52** (7), 1595–1625.

17 G.F. Oster, J.D. Murray and A.K. Harris (1983). Mechanical aspects of mesenchymal morphogenesis. *J Embryol. exp. Morph.*, **78**, 83–125.

18 D. Manoussaki (2003). A mechanochemical model of angiogenesis and vasculogenesis. *Mathematical Modelling and Numerical Analysis*, **37** (4), 581–599.

19 P. Namy, J. Ohayon and P. Tracqui (2004). Critical conditions for pattern formation and in vitro tubulogenesis driven by cellular traction fields. *Journal of Theoretical Biology*, **227**, 103–120.

20 S. Ramtani (2004). Mechanical modelling of cell/ecm and cell/cell interactions during the contraction of a fibroblast-populated collagen microsphere: theory and model simulation. *J. Biomech.*, **37** (11), 1709–18.

21 C.J. Hernandez (2001). *Simulation of bone remodeling during the development and treatment of osteoporosis*. PhD thesis, Stanford University, Stanford, California.

22 R.B. Martin (2003). Fatigue microdamage as an essential element of bone mechanics and biology. *Calcified Tissue International*, **73** (2), 101–107.

23 C.H. Turner (2002). Biomechanics of bone: determinants of skeletal fragility and bone quality. *Osteoporos Int.*, **13** (2), 97–104.

24 J.A. Buckwalter (2002). Articular cartilage injuries. *Clin. Orthop.*, **402**, 21–37.

25 R.G. Breuls, C.V. Bouten, C.W. Oomens, D.L. Bader and F.P. Baaijens (2003). A theoretical analysis of damage evolution in skeletal muscle tissue with reference to pressure ulcer development. *J. Biomech. Eng.*, **125** (6), 902–909.

26 R.G. Breuls, C.V. Bouten, C.W. Oomens, D.L. Bader and F.P. Baaijens (2003). Compression induced cell damage in engineered muscle tissue: an in vitro model to study pressure ulcer aetiology. *Ann Biomed. Eng.*, **31** (11), 1357–1364.

27 J. Lemaitre and J.L. Chaboche (1990). *Mechanics of solid materials*. Cambridge University Press, Cambridge.

28 J.C. Simo and J.W. Ju (1987). Strain- and stress-based continuum damage models: I. formulation. *International Journal of Solids and Structures*, **23**, 821–840.

29 J.P. Cordebois and F. Sideroff (1982). Damage induced elastic anisotropy. *Mechanical Behavior of Anisotropic Solids. Proc. EUROMECH colloque*, **115**, 761–774.

30 D.B. Burr, C.H. Turner, P. Naick, M.R. Forwood, W. Ambrosius, M.S. Hasan and R. Pidaparti (1998). Does microdamage accumulation affect the mechanical properties of bone? *J. Biomech.*, **31** (4), 337–345.

31 J.E. Marsden and T.J.R. Hughes (1983). *Mathematical foundations of elasticity*. Dover Publications, INC., New York.

32 E.K. Rodriguez, A. Hoger and A.D. McCulloch (1994). Stress-dependent finite growth in soft elastic tissues. *J. Biomech.*, 27 (4), 455–467.

33 C. Truesdell and W. Noll (1965). *The Non-linear Field Theories, (Handbuch der Physik, Band III)*. Springer, Berlin.

34 J.D. Murray and G.F. Oster (1984). Cell traction models for generating pattern and form in morphogenesis. *J. Math. Biol.*, 19 (3), 265–279.

35 S. Harada and G.A. Rodan (2003). Control of osteoblast function and regulation of bone mass. *Nature*, **423**, 349–356.

36 H.M. Frost (1964). *Dynamics of bone remodelling*, pages 315–333. Bone biodynamics. Boston. Little, Brown Co..

37 S.J. Hazelwood, R.B. Martin, M.M. Rashid and J.J. Rodrigo (2001). A mechanistic model for internal bone remodeling exhibits different dynamic responses in disuse and overload? *J. Biomech.*, **34** (3), 299–308.

38 J. Wolff (1892). *The Law of Bone Remodelling*. Das Gesetz derTransformation der Knochen, Kirschwald. Translated by Maquet, P., Furlong, R.

39 R. Huiskes, H. Weinans, H.J. Grootenboer, M. Dalstra, B. Fudala and T.J. Sloof (1987). Adaptive bone-remodelling theory applied to prosthetic-design analysis. *J. Biomech.*, **20** (11/12), 1135–1150.

40 D.R. Carter, D.P. Fyhrie and R.T. Whalen (1987). Trabecular bone density and loading history: regulation of connective tissue biology by mechanical energy. *J. Biomech.*, **20** (8), 1095–1109.

41 P.J. Prendergast and D. Taylor (1994). Prediction of bone adaptation using damage accumulation. *J. Biomech.*, **27**, 1067–1076.

42 R.B. Martin (1995). A mathematical model for fatigue damage repair and stress fracture osteonal bone. *J. Orhop. Res.*, **13**, 309–316.

43 C.R. Jacobs, J.C. Simo, G.S. Beaupré and D.R. Carter (1997). Adaptive bone remodeling incorporating simultaneous density and anisotropy considerations. *J. Biomech.*, **30** (6), 603–13.

44 R.T. Hart and S.P. Fritton (1997). Introduction to finite element based simulation of functional adaptation of cancellous bone. *Forma*, **12**, 277–299.

45 P. Fernandes, H. Rodrigues and C.R. Jacobs (1999). A model of bone adaptation using a global optimisation criterion based on the trajectorial theory of wolff. *Comput. Methods Biomech. Biomed. Eng.*, **2** (2), 125–138.

46 M. Doblaré and J.M. García (2001). Application of an anisotropic bone-remodelling model based on a damage-repair theory to the analysis of the proximal femur before and after total hip replacement. *J. Biomech.*, **34** (9), 1157–70.

47 M. Doblaré and J.M. García (2002). Anisotropic bone remodelling model based on a continuum damage-repair theory. *J. Biomech.*, **35** (1), 1–17.

48 S.C. Cowin and D.H. Hegedus (1976). Bone remodeling i: A theory of adaptive elasticity. *J. Elasticity*, **6**, 313–326.

49 R.T. Hart, D.T. Davy and K.G. Heiple (1984). A computational model for stress analysis of adaptive elastic materials with a view toward applications in strain-induced bone remodelling. *J. Biomech. Eng.*, **106**, 342–350.

50 G.S. Beaupré, T.E. Orr and D.R. Carter (1990). An approach for time-dependent bone modeling and remodeling-theoretical development. *Journal of Orthopaedic Research*, **8**, 551–651.

51 H. Weinans, R. Huiskes and H.J. Grootenboer (1992). The behavior of adaptive bone-remodeling simulation models. *J. Biomech.*, **25**, 1425–1441.

52 S. Ramtani and M. Zidi (2001). A theoretical model of the effect of continuum damage on a bone adaptation model. *J. Biomech.*, **34** (4), 471–9.

53 R. Huiskes, R. Ruimerman, G.H. van Lenthe and J.D. Janssen (2000). Effects of mechanical forces on maintenance and adaptation of form in trabecular bone. *Nature*, **405**, 704–706.

54 C.J. Hernandez, G.S. Beaupré and D.R. Carter (2000). A model of mechanobiologic and metabolic influences on bone adaptation. *J. Rehabil. Res. Dev.*, **37** (2), 235–244.

55 C.J. Hernandez, G.S. Beaupré, R. Marcus and D.R. Carter (2001). A theoretical analysis of the contributions of remodeling space, mineralization, and bone balance to changes in bone mineral density during alendronate treatment. *Bone*, **29** (6), 511–516.

56 C.J. Hernandez, G.S. Beaupré and D.R. Carter (2003). A theoretical analysis of the changes in basic multicellular unit activity at menopause. *Bone*, **32**, 357–63.

57 R.B. Martin, D.B. Burr and N.A. Sharkey (1998). *Skeletal Tissue Mechanics*. New York: Springer-Verlarg.

58 R.B. Martin (1984). *Porosity and specific surface of bone*, volume 10 of *Critical Reviews in Biomedical Engineering*, Chapter 3, pp. 179–222. CRC Press.

59 C.J. Hernández, G.S. Beaupré, T.S. Keller, and D.R. Carter (2001). The influence of bone volume fraction and ash fraction on bone strength and modulus. *Bone*, **29** (1), 74–78.

60 C.A. Pattin, W.E. Caler and D.R. Carter (1996). Cyclic mechanical property degradation during fatigue loading of cortical bone. *J Biomech*, **29** (1), 69–79.

61 P.K. Venesmaa, H.P. Kroger, J.S. Jurvelin, H.J. Miettinen, O.T. Suomalainen and E.M. Alhava (2003). Periprosthetic bone loss after cemented total hip arthroplasty: a prospective 5-year dual energy radiographic absorptiometry study of 15 patients. *Acta Orthop. Scand.*, **74** (1), 31–36.

62 D.E. Ashhurst (1986). The influence of mechanical stability on the healing of experimental fractures in the rabbit: a microscopical study. Series B **313**, 271–302.

63 M.M. Sandberg, H.T. Aro and E. I. Vuorio (1993). Gene expression during bone repair. *Clin. Orthop. Rel. Res.*

64 F. Pauwels (1960). Eine neue theorie über den einflub mechanischer reize auf die differenzierung der stützgewebe. *Z. Anat. Entwicklungsgeschichte*, **121**, 478–515.

65 S.M. Perren (1979). Physical and biological aspects of fracture healing with special reference to internal fixation. *Clin. Orthop. Rel. Res.*, **138**, 175–196.

66 S.M. Perren and J. Cordey (1980). *The concept of interfragmentary strain*, pp. 63–77. Currect concepts of internal fixation of fractures. Springer-Verlarg, Berlin.

67 D.R. Carter, P.R. Blenman and G.S. Beaupré (1998). Correlations between mechanical stress history and tissue differentiation in initial fracture healing. *J. Orthop. Res.*, **6**, 736–748.

68 D.R. Carter, G.S. Beaupré, N.J. Giori and J.A. Helms (1998). Mechanobiology of skeletal regeneration. *Clin. Orthop. Rel. Res.*, **S355**, S41–S55.

69 L.E. Claes and C.A. Heigele (1999). Magnitudes of local stress and strain along bony surfaces predict the course and type of fracture healing. *J. Biomech.*, 32:255–266, 1999.

70 P.J. Prendergast, R. Huiskes and K. Soballe (1997). Biophysical stimuli on cells during tissue differentiation at implant interfaces. *J. Biomech.*, **6**, 539–548.

71 A. Bailón-Plaza and M.C.H. Van Der Meulen (2001). A mathematical framework to study the effects of growth factor influences on fracture healing. *J. Theor. Biol.*, **212**, 191–209.

72 D. Lacroix and P.J. Prendergast (2002). A mechano-regulation model for tissue differentiation during fracture healing: analysis of gap size and loading. *J. Biomech.*, **35**, 1163–1171.

73 U. Simon, P. Augat, M. Utz and L. Claes (2002). Dynamical simulation of the fracture healing process including vascularity. *Acta of Bioengineering and Biomechanics*, **4 S1**, 772–773.

74 A. Bailón-Plaza and M.C.H. van der Meulen (2003). A Mathematical Framework to Study the Effects of Growth Factor Influences on Fracture Healing . *Journal of Biomechanics*, **36**, 1069–1077.

75 J.H. Kuiper, J.B. Richardson and B.A. Ashton (2000). Computer simulation to study the effect of fracture site movement on tissue formation and fracture stiffness restoration. In *European Congress on Computational Methods in Applied Sciences and Engineering ECCOMAS*.

76 Ch. Ament and E.P. Hofer (2000). A fuzzy logic model of fracture healing . *J. Biomech.*, **33**, 961–968.

77 M.J. Gómez-Benito, J.M. García-Aznar, J.H. Kuiper, M. Doblaré and J.B. Richardson (2005). Influence of fracture gap size on the pattern of long bone healing: A computational study. *J Theor Biol*, **235** (1), 105–119.

78 J.H. Kuiper, J.B. Richardson and B.A. Ashton (1996). Mechanical signals in early fracture callus. In J. Vander Sloten, G. Lowet, R. Van Audekercke, and G. Van der Perre, editors, *Proc 10th Europ Soc Biomech*, page 154.

79 J.H. Kuiper, B.A. Ashton and J.B. Richardson (2000). Computer simulation of fracture callus formation and stiffness restoration. In P.J. Prendergast, T.C. Lee, and A.J. Carr (Eds.), *Proc 12th Europ Soc Biomech*, page 61.

80 D. Lacroix (2000). *Simulation of tissue differentiation during fracture healing.* PhD thesis, University of Dublin.

81 D.M. Cullinane, K.T. Salisbury, Y. Alkhiary and S. Eisenberg (2003). Effects of the local mechanical environtment on vertebrate tissue differentiation during repair: does repair recapitulate development. *The Journal of Experimental Biology*, **206**, 2459–2471.

82 G.S. Beaupré, T.E. Orr and D.R. Carter (1990). An approach for time-dependent bone modeling and remodeling-application: A preliminary remodeling simulation. *Journal of Orthopaedic Research*, **8**, 662–670.

83 G.J. Breur, VanEnkevort, C.E. Farnum and N.J. Wilsman (1991). Linear Relationship between the Volume of Hypertrophic Chondrocytes and the Rate of Longitudinal Bone Growth in Growth Plates. *Journal of Orthopeadic Research*, **9**, 348–359.

84 N.J. Wilsman, C.E. Farnum, E.M. Leiferman, M. Fry and C. Barreto (1996). Differential growth by growth plates as a function of multiple parameters of chondrocytic kinetics. *Journal of Orthopaedic Research*, **14**, 927–936.

85 Ch. Ament and E.P. Hofer (1996). On the importance of the osteogenic and vasculative factors in callus healing. In *Proc. of the 5th Meeting of the International Society for Fracture Repair.*

86 C.R. Jacobs (1994). *Numerical simulation of Bone Adaptation to Mechanical Loading.* PhD thesis, Stanford University.

87 J.R. Levick (1987). Flow through interstitium and other fibrous matrices. *Quaterly Journal of Experimental Physiology*, **72**, 409–438.

88 E. Mücke (1993). *Shapes and Implementations in Three-Dimensional Geometry.* PhD thesis, University of Illinois at Urbana-Champaign.

89 L. Claes, P. Augat, G. Suger and H.J. Wilke (1997). Influence of size and stability of the osteotomy gap on the success of fracture healing. *J. Orthop. Res.*, **15** (4), 577–584.

90 H.M. Frost (1988). The biology of fracture healing. *Clinical Orhopaedics and Related Research*, **248**, 283–293.

91 R. Dillon and H.G. Othmer (1999). A mathematical model for outgrowth and spatial patterning of the vertebrate limb bud. *Journal of Theoretical Biology*, **197** (3), 295–330.

Please address your comments or questions on this paper to:
International Center for Numerical Methods in Engineering
Edificio C-1, Campus Norte UPC
Grand Capitán s/n
08034 Barcelona, Spain
Phone: 34-93-4016035; Fax: 34-93-4016517
E-mail: onate@cimne.upc.edu